EFFECTS OF DEGENERACIES ON SELF-INDUCED TRANSPARENCY

by

GREGORY JOSEPH SALAMO

A dissertation submitted to the Graduate Faculty in Physics in partial fulfillment of the requirements for the degree of Doctor of Philosophy, The City University of New York.

1974

This manuscript has been read and accepted for the Graduate Faculty in Physics in satisfaction of the dissertation requirement for the degree of Doctor of Philosophy.

Hyatt M. Gibbs

1-25-74
date

George Skorinko HMG
Chairman of Examining Committee

1-29-74
date

Marvin H. Mittleman
Executive Officer

Samuel L. McCall
Sam McCall

Joseph Krieger

Melnn Lax

Supervisory Committee

The City University of New York

Acknowledgments

I would like to thank Hyatt M. Gibbs for he contributed most to my development as an experimentalist. I would also like to thank him for his sincere and honest friendship during this work.

I thank George G. Churchill whose contribution and efforts to the development of the apparatus and experiment were great and with whom working was a pleasure.

I would like to thank my wife Jacqueline, who during this work gave to me the most important thing of all, love and understanding. I dedicate this work to my son Paul and my little girl Melody, who provided the daily joy in my life.

I should also like to thank the faculty of Brooklyn College who I believe gave to me the most fulfilling and enjoyable education. In particular, I would like to thank Professor George Skorinko, Professor Alvin M. Halpern, Professor John Dooley, and Professor Louis S. Celenza, who it seemed at any hour of any day helped me through most of my course work. A special thanks to Professor George Skorinko for guiding my studies through school and helping with all kinds of problems.

I would like to thank Dr. Samuel L. McCall who helped greatly in analyzing the data using the pulse-area-pulse-energy approach.

I would like to thank Professor Narkis Tzoar at City College for an interesting presentation of solid state theory.

It is a pleasure to also acknowledge several helpful conversations with Dr. Eric Ippen of Bell Laboratories on the operation and construction of dye lasers.

A special thanks to Miss Patricia A. Murray for typing the final draft of this thesis.

Finally, I would like to acknowledge financial support from Brooklyn College, and to a smaller degree, Bell Laboratories, which made this thesis possible.

Table of Contents

List of Tables

List of Figures

I. Introduction

When a group of atoms is coherently excited by a short optical pulse, a macroscopic polarization is induced. This polarization will then add coherently to the driving electric field and reshape the pulse. The evolution of the system can be described by a self-consistent solution of Schrodinger's equation, which describes the induced polarization, and Maxwell's equations, which describe the effect of the induced polarization on the pulse. This simultaneous solution constitutes the state of self-induced transparency (SIT) first described and observed by S. L. McCall and E. L. Hahn.[1]

Since the initial observations of self-induced transparency in ruby[1] and SF_6,[2] experiments have continued to show remarkable agreement between theory and experiment. In particular, observations of peak intensity amplification and pulse breakup in a simple atomic system,[3] which were compared with computer simulation, have clearly demonstrated the accuracy of the McCall-Hahn description of this coherent optical effect.

This thesis describes the observation of SIT using a C. W. dye laser and sodium vapor. We have studied for the first time SIT in a degenerate system with clearly defined transition dipole moments. Due to Doppler broadening in Na, the dye laser, tuned to either the D_1 or the D_2

transition, excites many transition dipoles even in the presence of large magnetic fields. For small magnetic fields of 60 to 150 Gauss, many of these excited transitions have different dipole moments and it therefore becomes possible to study SIT when several different transition dipoles are excited. Since several different two level systems are excited by the optical pulse, this will be referred to as the degenerate case. This experiment demonstrates, in this case, that although the degeneracy does diminish the features of SIT, all of the characteristics including pulse breakup are still observed. If the magnetic field is increased to 2 or 3 kilogauss, the excited transitions have exactly the same transition dipole moment and the degeneracy should in no way affect the characteristics of SIT. Experimental results are in complete agreement with this expectation. Since the optical pulse excites identical two level systems, this is referred to as the nondegenerate case. The dye laser - Na experiment therefore provides a system which by simple adjustment of the magnetic field can be converted from a system with identical transition dipole moments to a system with several different transition dipole moments. In this way a direct comparison can be made between the two cases and the effect of exciting several different clearly defined transition dipole moments on the features of SIT may be identified. As the magnetic field is lowered to zero an interesting thing happens. If the hyperfine energy splitting is greater than $\frac{\hbar}{\tau_p}$, where τ_p is the width in time of the optical pulse, as is the case for the D_1

transition in Na, each transition is distinct. Therefore, several different dipoles are excited and the system is the same as the case for low magnetic fields of 60 to 150 Gauss. However, for the D_2 transition in Na the hyperfine energy splitting is less than $\frac{\hbar}{\tau_p}$ and transitions are not distinct. In this case a representation can be chosen in which transitions are independent of one another. In this representation each transition has exactly the same dipole moment and the characteristics of SIT are expected to be unaffected by the degeneracy as was observed experimentally.

In addition to investigation of degeneracy effects on the characteristics of SIT this experiment demonstrates for the first time[4] that a C.W. dye laser can be used to study coherent optical effects. The results from the dye laser - Na system are in fact as clear a demonstration of SIT as any previous experimental results, and this system has the additional advantage of not requiring the expense and inconvenience of a superconducting magnet to bring the laser and absorber into coincidence.[3] In this way this experiment could stimulate further coherent optics experiments on a similar system. This is especially true today since dye lasers, offering the promise of a versatile tool, can now be found in many laboratories. In addition, since C.W. dye lasers are now tunable over a large bandwidth, many of the potential uses of SIT[3] and other related phenomena (photon echoes[5] and optical nutations[6]) are now closer to reality. An example of this can be seen in the Na experiment. SIT

phenomena were studied on both the D_1 and D_2 transitions in sodium. For light linearly polarized parallel to a large magnetic field with the propagation vector perpendicular to the field the same input pulse was seen to correspond to an output area of about 6π for the D_2 transition but closer to 4π for the D_1 transition. This observation is in agreement with theory since the dipole moment of the D_2 transition is a factor of $\sqrt{2}$ larger than the dipole moment of the D_1 transition. Similar results were seen for light circularly polarized along the magnetic field. In this case the transition dipole of the $^2S_{1/2}(M_J=1/2)$ to $^2P_{3/2}(M_J=3/2)$ transition is a factor of the $\sqrt{3}$ larger than the transition dipole of the $^2S_{1/2}(M_J=-1/2)$ to $^2P_{3/2}(M_J=1/2)$ transition and a factor of the $\sqrt{\frac{3}{2}}$ larger than the transition dipole of the $^2S_{1/2}(M_J=-1/2)$ to $^2P_{1/2}(M_J=+1/2)$ transition. For the same intensity input pulse the output pulse was seen to correspond in area to 6π for the $^2S_{1/2}(M_J=1/2)$ to $^2P(M_J=3/2)$ transition, 3π for the $^2S_{1/2}(M_J=-1/2)$ to $^2P_{3/2}(M_J=1/2)$ transition, and 4π for the $^2S_{1/2}(M_J=-1/2)$ to $^2P_{1/2}(M_J=1/2)$ transition. This is an indication that it may be possible to measure relative dipole strengths for different transitions using a tunable dye laser and SIT phenomena.

Experimental results for the case of identical excited transition dipoles include a clear demonstration of pulse break-up, peak intensity amplification, pulse delays, and nonlinear transmission. These results were found to be nearly the same as a previous Rb experiment[3] where comparison

between theory and experiment was shown to be excellent. Therefore, there is good agreement between theory and experiment for Na also. In addition, the case in which different transition dipoles are excited is found to be described qualitatively using the pulse-area-pulse-energy description of McCall and Hahn.[7]

Footnotes

1. (a) S. L. McCall and E. L. Hahn, Phys. Rev. Lett. 18, 908 (1967); (b) Phys. Rev. 183, 457 (1969).

2. C. K. N. Patel and R. E. Slusher, Phys. Rev. Lett. 19, 1019 (1967).

3. (a) H. M. Gibbs and R. E. Slusher, Phys. Rev. Lett. 24, 638 (1970); (b) Phys. Rev. A 5, 1634 (1972).

4. Self-induced transparency using a dye laser was reported by D. J. Bradley, G. M. Gale, and P. D. Smith, Nature 225, 719 (1970). However, the distinguishing characteristics of peak amplification and pulse breakup were not observed.

5. I. D. Abella, N. A. Kurnit and S. R. Hartmann, Phys. Rev. 141, 391 (1966).

6. G. B. Hocker and C. L. Tang, Phys. Rev. 184, 356 (1969); H. M. Gibbs, Phys. Rev. A 8, 446 (1973).

7. S. L. McCall and E. L. Hahn, Phys. Rev. A 2, 861 (1970).

II. Experimental Apparatus

The basic apparatus used in our investigations is shown in Fig. 1. A Coherent Radiation 53B argon laser was used to pump a Rhodamine 6G tunable C.W. dye laser. The dye laser was constructed using a cavity design first introduced by Dienes, Ippen, and Shank.[8] The output of the dye laser was then gated through a Glans prism (GP) by a Pockels cell (PC) at the rate of 100 pps.[3] This resulted in 5 nsec pulses which were focused by a lens (L_1) into a 2-mm sodium cell (Na). The sodium cell was housed in an oven and placed in a magnetic field which could be varied from zero to eight kilogauss. A lens (L_2) was used to image the excited region in the cell onto an aperture (A_3) in order to select only the uniform-plane-wave excited region for observation. The output from the aperture was then focused by a third lens (L_3) onto a fast detector (D_1) and then displayed on a fast 7904 Tektronix oscilloscope. The frequency profile of the dye laser was continuously monitored by a scanning Fabry-Perot interferometer.

The remainder of this section is devoted to a more detailed description of the apparatus.

A. Dye Laser Construction

The dye laser cavity configuration is shown in Fig. 2. The astigmatically compensated cavity design was first

introduced to dye lasers by Dienes, Ippen and Shank.[8] The cavity consisted of three mirrors (M_1,M_2,M_3) and one Brewster angle prism (P). The Rhodamine 6G dye was pumped by the argon laser beam which entered the cavity through the prism and was focused by the 10 cm mirror (M_3) into the dye cell to a beam diameter of about 30μm.

Astigmatic compensation can be achieved with this cavity design since the astigmatism produced due to the angle of incidence at mirror M_3 can be compensated by the astigmatism produced due to focusing into the Brewster-angle dye cell. An analysis of the folded three-mirror cavity has been performed by Kogelnik, Ippen, Dienes and Shank using imaging rules.[9] This analysis yields equations for quantities of interest, such as, the stability range, the size and location of the beam waist, and the angle θ necessary to achieve astigmatic compensation. These equations are:

$$\text{Stability range} \equiv 2S = \frac{f^2}{d_2} \qquad (1)$$

where d_2 is the separation between R_2 and R_3 while $f \equiv \frac{R_3}{2}$. The stability range can be adjusted by varying the separation between R_1 and R_3 from

$$d_1(\text{max}) = R_1 + f + 2S \qquad (2)$$

to

$$d_1(\text{min}) = R_1 + f.$$

In the stability-range center the beam waist deviates very little from R_1. This deviation is given by

$$t_1 = \frac{S^2}{R_1} . \tag{3}$$

The confocal parameter b is

$$b \equiv \frac{2\pi W_0^2}{\lambda} = 2S \tag{4}$$

where W_0 is the radius of the beam waist and λ is the wave length of light in the cavity. The angle θ necessary to achieve astigmatic compensation can be found from the equation

$$\frac{(n^2-1)t\sqrt{n^2+1}}{n^4} = f \sin\theta \tan\theta \tag{5}$$

where n is the index of refraction and t is the thickness of the dye cell. The parameters for our dye laser cavity were, $R_1 = 5\text{cm}$, $f = \frac{R_3}{2} = 5\text{cm}$, $R_2 = \infty$, $d_2 = 100\text{cm}$, $t \simeq 1.5\text{mm}$, and $n \approx 1.5$ for both the dye solution and for the glass windows. Therefore, our cavity had a stability range of $2S = 2.5\text{mm}$, $t_1 = 31\mu$, $2W_0 = 31\mu$, and $\theta \simeq 7°$.

The dye laser was initially operated with the cavity adjusted near the middle of the stability range. For this configuration the output of the dye laser was about 4A° wide and modulated in amplitude at a μ-sec rate. Both characteristics were much improved by placing an aperture at mirror M_2 and operating near the edge of the stability range corresponding to the largest M_1 to M_3 separation ($d_1(\text{max}) = f+R_1+2S$).

Under these conditions, the spectral output of the laser was reduced to about .5A° and the μ-sec amplitude modulation was lowered to a few percent. Attempts to use the aperture when the cavity was adjusted to the middle or other end of the stability range also resulted in a reduction in the spectral output. However, this was accompanied by a severe reduction in output power. Therefore, for our experiment, the cavity was adjusted near the edge of the stability range corresponding to $d_1 = d_1(\max)$. Occasionally, lasing would occur along several paths in the cavity simultaneously. This problem was also eliminated by the presence of the aperture near M_1. The more desirable characteristics found when operating with the cavity configuration corresponding to the larger separation between M_1 and M_3 ($d_1=d_1(\max)$) can perhaps be explained by examining the lowest-order mode of the cavity as a function of the stability range. When the cavity is adjusted near the edge of the stability range where $d_1 = d_1(\max)$, the lowest order cavity mode is such that the dye laser beam is focused on M_2 (Fig. 3a). On the other hand, when the cavity is adjusted to the other end of the stability range where $d_1 = d_1(\min)$, the dye laser beam is parallel at M_2 (Fig 3b). In addition we should keep in mind the experimental observation that lasing can occur along several paths simultaneously and each at a different wave length. In Fig. 3a lasing along another path can occur only if that path, in the short leg of the cavity, is shorter than shown since we are on the stability edge where $d_1 = d_1(\max)$. This

would mean that the mode along the additional optical path would not be focused on mirror M_2 and would not lase due to the aperture at M_2. On the other hand, in Fig. 3b, lasing along another path can occur only if the path in the short leg of the cavity is longer than shown since $d_1 = d_1(\text{min})$. Therefore the mode along the additional optical path would tend to be focused on M_2 and not prevented from lasing by the aperture. If the aperture is closed down tight in an effort to prevent unwanted modes from lasing, power would be lost from the dominant mode.

The only disadvantage of operating on the stability edge where $d_1 = d_1(\text{max})$ was that the output of the dye laser was astigmatically distorted. This was perhaps due to the fact that compensation becomes very critical at the edge of the stability range. For example, the cavity could be stable in the vertical plane (tangential rays) but at the near edge of the stability range in the horizontal plane (sagittal rays). In addition, as was mentioned previously, at this edge of the stability range the cavity mode is focused on mirror M_2. This means that the cavity mode is also focused through the Brewster-angle prism and therefore could give rise to a further astigmatic distortion similar to that caused by focusing into the Brewster-angle dye cell. Therefore, in scanning through the stability range the angle θ for astigmatic correction would have to be changed.

In order to operate the dye laser on the edge of the stability range where $d_1 = d_1(\text{max})$, it was necessary to use

a lens (L_4) to focus the argon laser beam near M_1, as shown in Fig. 2. In this way, the argon beam waist is moved out about 2.5cm beyond the focal point of mirror M_3 which is also the location of the dye waist on this edge of the stability range. It was expected that this would also more closely mode match the two waists since the dye laser is also focused at mirror M_1 on this edge of the stability range. At the other edge the dye waist is located at the focal point of M_3. For operation on this edge of the stability range the lens would have to be removed so that the argon waist could be moved closer to the focal point of M_3.

The dye laser was rigidly held together by the use of Cervit rods which have a low thermal coefficient of expansion. In addition, in order to minimize vibrations, both the dye laser and argon laser were mounted on a slab of aluminum which was floated on four Firestone 110B tires.

B. Dye and Circulating System

The circulating system for the Rhodamine 6G dye is shown in Fig. 4. The dye was dissolved in a solution of distilled water and 5% (by vol.) Ammonyx-LO. The concentration of the solution was about 2×10^{-4} molar. Higher concentrations were found to lead to thermal deterioration of the dye-cell windows. The dye was circulated by a micropump model 1284 V pump through the Millipore filter, the buffer reservoir, and on through the cell. With an input pressure of about 70 psi the dye velocity in the cell was about 18 m/sec.

Inert cobothane tubing was used to flow the dye while stainless steel and copper fittings were used to couple sections together. It was found necessary to use a restriction at the output of the circulating system in order to prevent cavitation from occurring inside the dye cell. The use of the restriction reduced the spectral output of the dye laser from typically 100 MHz to 20 MHz and improved the frequency stability of the laser.

C. Dye Cell and Windows

Several types of dye cells were tried, some of which are shown in Fig. 5. Of those shown it was found that the cells with the short 6mm flow path (cells A and B) worked best. The shorter path allowed a high velocity which was necessary to prevent thermal problems. Experimentally, no distinction was noticed between cells A and B which were designed to give turbulent and laminar flow, respectively.

Several types of windows were also tried, all of which were 0.25mm thick. Fused quartz windows worked well, but it was found that Corning glass cover slips were cheaper and had similar optical quality. Sapphire windows were tried once but poor optical quality resulted in low output laser power and thus discouraged further efforts. All windows were epoxyed on with Torr Seal (made by Varian).

D. Single Longitudinal Mode

As mentioned previously the spectral output of the dye laser was about 40 GHz. The longitudinal modes of the

1 meter cavity were about 150 MHz apart. Single mode operation was achieved with the addition of three etalons into the cavity. The first etalon was a Corning cover slip 250μm thick corresponding to a spectral range of 400 GHz. This etalon narrowed the spectral output to about 25 GHz indicating a finesse of 16. That such a high finesse is possible from an uncoated etalon is related to the multiple passes which occur in the laser cavity. The effective finesse in a laser cavity is N times the finesse of the etalon outside the cavity, where N is the average number of round trips a photon makes in the cavity. The spectral output of the laser was then reduced to about 2.5 GHz by adding a second etalon 3mm thick having a free spectral range of about 33 GHz. The finesse of this etalon was therefore about 13. The addttion of a second etalon increases the cavity loss per pass and therefore lowers the round trip number N. This explains why the effective finesse of the second etalon was less than 16. It also explains the experimental observation that when an additional etalon is added to a cavity the finesse of preceding etalons is found to diminish. Finally, a 1 cm etalon was added which had a reflective coating of 20% on each side. This etalon generally selected a single mode although sometimes two cavity modes oscillated simultaneously. This indicates that the etalon actually limited the spectral output to about 150 MHz. Therefore, the free spectral range of the 1 cm etalon was 10 GHz and its effective finesse about 66. This higher

finesse was due to the 20% coating. The actual spectral width of the single longitudinal mode was 20 MHz. Figure 6 shows the reduction in the frequency profile with the addition of each etalon.

Although the last etalon selects a single cavity mode, it is the finesse of the cavity itself which ultimately determines the width of the cavity mode and the spectral width of the dye laser. The finesse of the cavity is limited by such things as mechanical stability, air currents, and temperature changes. These factors are in general common to all laser cavities and are dealt with in a straightforward way. However, the dye laser has the additional optical path instabilities due to the dye cell. Thermal effects and cavitation are very detrimental to narrowline operation of the dye laser. High dye velocities are necessary to prevent thermal effects and a restriction at the output of the circulating system (see II-B) is necessary to prevent cavitation.

E. Dye Laser Tuning and Alignment

The output of the dye laser was monitored by a scanning Fabry-Perot interferometer (FP_1). The free spectral range (FSR) of the Fabry-Perot was 3 GHz and the finesse was better than 100. This Fabry-Perot was used to obtain information on the spectral width of the single longitudinal mode and for fine tuning. In addition, it was found convenient to use a second Fabry-Perot (FP_2), with a larger FSR of 60 GHz and a finesse of about 20 in order to monitor the

spectral output of the laser before and after inserting etalons into the cavity. For example, the laser was tuned to the D_1 absorption line in Na by tilting mirror M_2 until fluorescence was seen in the Osram Lamp (O_1) which was not excited electrically but was heated by heater tape. Comparison of the laser output with an electrically excited Osram Lamp (O_2) through spectrometer (S) made it easy to distinguish the D_1 line from the D_2 line. The 250μm etalon was then inserted into the cavity and tilted slightly until fluorescence could again be seen in the heated Osram Lamp. The 3mm etalon was then added and tilted to tune the laser back on to the D_1 line. In general, the laser would oscillate in two modes of the 3mm etalon and required further tilting of the 250μm etalon to be corrected. During this time the Fabry-Perot (FP_2), which was calibrated with respect to the fluorescence from the heated Osram Lamp, provided a visual picture of the effect of tilting and inserting each etalon. It therefore indicated which etalon should be tilted to correct a milti-mode problem and also indicated how much tilt was required to find resonance. Finally, the 1cm etalon was added followed by retuning to the D_1 line by tilting each etalon while observing the Fabry-Perot (FP_2) and the fluorescence from the Osram Lamp. Fine tuning of the laser in discrete steps of 150 MHz was accomplished by heating the 1cm etalon followed by slight tilt adjustments on the 3mm and 250μm etalons to keep the laser in a single longitudinal mode.

F. Comparison With Ideal Optical Pulse

In an attempt to satisfy the uniform plane wave condition and have sufficient power for 4π pulses, the dye laser was focused by a long focal length lens (38cm) to a diameter of about 75μm into a short Na cell (2mm). Diffraction effects should be negligible since $\frac{a^2}{b\lambda} > 1$. In addition, the focal region was imaged by a lens onto a 100μm aperture as shown in Fig. 7. Since the image of the focal region was magnified by a factor of 3, the aperture selected a fraction of the focal region which was nearly uniform in intensity for observation. Care was taken to choose a lens with resolution capable of resolving the uniform-plane-wave region. The focal region in the Na cell can be estimated by measuring the size of the image at the aperture. In our experiment the cross-section of the image was 163μm by 288μm. The cross-section of the output beam of the dye laser was approximately 6mm by 2.5mm. An aperture was used A_2 (Fig. 1) which improved this to about 4mm by 2.5. The expected diffraction limited beam waist from a rectangular aperture is then 70μm by 90μm which agrees with the experimental value of 54μm by 99μm. The peak power of the light pulse was measured to be about 4mW which gives an average peak intensity of about 80 W/cm^2. The intensity necessary for a 2π pulse can be estimated by (see Sec. III-B)

$$\frac{2p}{\hbar}\int_{-\infty}^{\infty} \mathcal{E}dt \simeq \frac{2p}{\hbar}\,\mathcal{E}_{max}\,\tau_p = 2\pi$$

$$I = \frac{c\left|\mathcal{E}_{max}\right|^2}{4\pi} = \frac{c\pi\hbar^2}{4p^2\tau_p^2} = 7.7\ \mathrm{W/cm^2}. \qquad (6)$$

Therefore, there was enough intensity for 6π pulses which were clearly observed.

Footnotes

8. A. Dienes, E. P. Ippen, and C. V. Shank, IEEE J. Quantum Electronics QE-8, 388 (1972).

9. H. Kogelnik, E. P. Ippen, A. Dienes, and C. V. Shank, IEEE J. Quantum Electronics QE-8, 373 (1972).

III. Atomic Absorber

An energy level diagram of sodium as a function of magnetic field is shown in Fig. 8. In a strong magnetic field the nuclear spin I and the electronic angular momentum J are decoupled so that the good quantum numbers for the system are J, M_J, I, and M_I. In this case, the separation between M_I sublevels is 443 MHz (Sec. III-B) for the ground state $^2S_{1/2}$ and less than 50 MHz for the M_I sublevels of the $^2P_{1/2}$ and the $^2P_{3/2}$ excited states. As a result of the 1.7 GHz Doppler width allowed transitions between $|JM_JIM_I\rangle$ ground states of the same JM_JI but different M_I and excited states $|J'M_JIM_I\rangle$ of the same J', M_J, I but different M_I are not resolved. However, the transition electric dipole moment is the same for any allowed transition between M_I sublevels of the ground state $^2S_{1/2}(M_J=1/2)$ (or $^2S_{1/2}(M_J=-1/2)$) to sublevels of an excited state $^2P_{1/2}(M_J=1/2)$ (or $^2P_{1/2}(M_J=-1/2)$). Therefore, although a M_I degeneracy does exist, the excited dipoles are exactly the same and the characteristics of SIT should be unaffected. As was stated before we shall refer to this case in which identical dipoles are excited as the nondegenerate case.

On the other hand, in weak magnetic fields, the good quantum numbers are I, J, F, M_F. In this case, the transition dipole moments from a $|FM_F\rangle$ ground state to a $|F'M_F'\rangle$ excited

state can be and in general are different for different $|F'M_F'\rangle$. Therefore, the degeneracy due to overlapping transitions allows states with different transition dipole moments to be excited by the optical pulse. This is referred to as the degenerate case. The question then to which this thesis is directed is: will this degeneracy in general destroy the characteristics of SIT? The answer to this question is: no. Only in special cases was excitation of several different transition dipoles found to diminish the characteristic features of SIT. For example, for the D_1 degenerate case, all of the characteristic features of SIT were seen to be similar to the nondegenerate case. However, for the D_2 degenerate case, although nonlinear transmission and long delays were found similar to the nondegenerate case, the characteristic features of peaking and breakup were seen to be greatly diminished. These results can be explained on the basis of the relative value of the excited transition dipoles (Sec. V).

After a short discussion of the hyperfine structure of Na we proceed to calculate the electric dipole moments for the allowed transitions in the limit of large magnetic field (Sec. III-B) and in the limit of low magnetic field (Sec. III-C). The reader who is not interested in the transition dipole moment calculation and the corresponding intensity calculation for 2π area pulses may proceed to Section IV where the pulse-area-pulse-energy approach is described.

A. Hyperfine Structure of Na

An energy level diagram showing the hyperfine structure of Na is shown in Fig. 9. The Hamiltonian including the hyperfine interaction may be written as

$$\mathcal{H} = \mathcal{H}_0 + \text{ha } \mathbf{I}\cdot\mathbf{J} \tag{7}$$

where $\mathcal{H}_0$ is the Hamiltonian without the hyperfine interaction, h is Planck's constant, I the nuclear spin, J the electronic angular momentum, and "a" a number dependent on I and J. The eigenstates for the system can be represented as $|I,J,F,M_F\rangle$ where F is the total angular momentum and M_F the azimuthal component. In this representation the energy change due to the hyperfine interaction is given by[10]

$$W(F) = \langle FM_F IJ|haI\cdot J|FM_F IJ\rangle = [ha/2]\,[F(F+1)-I(I+1)-J(J+1)]. \tag{8}$$

The dependence of this expression on F indicates that states of same I and J but different F have different energy eigenvalues. However, states with same F, I, and J, but different M_F do have the same energy eigenvalues. The energy difference between states $|FM_F IJ\rangle$ and $|(F-1)M_F IJ\rangle$ is given by[10]

$$W(F) - W(F-1) = haF,$$
$$\text{or } \Delta\nu_{HF} = aF. \tag{9}$$

Experimental determination of $\Delta\nu_{HF}$ will then yield the quantity "a" which is a function of I and J but not F and M_F.

For sodium the hyperfine energy separation of the $^2S_{1/2}$ ground state is 1772 MHz and 192 MHz for the $^2P_{1/2}$ excited state.[11] The $^2P_{3/2}$ state has components F = 3,2,1,0. The hyperfine energy separations for these states are 60, 35, and 19 MHz, respectively.[12] The number "a" can now be determined and will be used to calculate the energy separation of M_I sublevels of a given M_J state at large magnetic fields.

B. Strong Magnetic Field

In a strong magnetic field the magnetic dipole energy for the state specified by $M_I M_J$ is given by[10]

$$W(M_I M_J) = - \frac{M_J H_0 M_J}{J} - \frac{M_I H_0 M_I}{I} + haM_I M_J. \qquad (10)$$

For the $^2S_{1/2}$ ground state the separation between levels of different M_I but same M_J is therefore approximately given by

$$\Delta W = ha(\Delta M_I)M_J, \qquad (11)$$

where "a" was shown to be $\frac{\Delta\nu_{HF}}{F}$. For the values $M_J = \pm 1/2$, $\Delta M_I = 1$

$$\Delta W = \frac{h\Delta\nu_{HF}}{2}\left(\frac{1}{2}\right) = \frac{h\Delta\nu_{HF}}{4},$$

so that

$$\frac{\Delta W}{h} = \frac{\Delta\nu_{HF}}{4} = \frac{1772}{4} = 443 \text{ MHz}. \qquad (12)$$

Similarly for the $^2P_{1/2}$, $M_J = \pm 1/2$

$$\frac{\Delta W}{h} = \frac{\Delta\nu_{HF}}{2}\left(\frac{1}{2}\right) = \frac{192}{4} = 48 \text{ MHz}. \tag{13}$$

For the $^2P_{3/2}$, $M_J = \pm 1/2$

$$\frac{\Delta W}{h} = \frac{\Delta\nu_{HF}}{2}\left(\frac{1}{2}\right) = \frac{35}{4} = 8.8 \text{ MHz}, \tag{14}$$

while for $M_J = \pm 3/2$

$$\frac{\Delta W}{h} = \frac{\Delta\nu_{HF}}{2}\left(\frac{3}{2}\right) = 26.3 \text{ MHz}. \tag{15}$$

In the Na-dye laser experiment, Na was heated to temperatures around 200° C. At these temperatures the Na Doppler width[13]

$$\Delta\nu_D = \frac{2\sqrt{2R\ell n2}}{c}\nu_0\sqrt{\frac{T}{M}} \tag{16}$$

is then about 1700 MHz. Therefore, transitions for different M_I between the ground state $|J,M_J,I,M_I\rangle$ and the excited state $|J',M_J,I,M_I\rangle$ are separated in frequency by only 1/3 of a Doppler width and are therefore unresolved.

For light linearly polarized parallel to the magnetic field and the wave vector perpendicular to the field the allowed transitions correspond to $\Delta M_J = 0$. The dipole moment of such transitions can be found from the lifetime of the excited state.[3] For example, the $^2P_{3/2}(M_J=-1/2,M_I=3/2)$ excited state $|a\rangle$ can make a transition to the $^2S_{1/2}$ $(M_J=-1/2,M_I=3/2)$ state $|b\rangle$ or to the $^2S_{1/2}(M_J=1/2,M_I=3/2)$ state $|c\rangle$. The ratio of the partial lifetimes of the excited

state can be found by application of the Wigner Eckart theorem[14] giving

$$\frac{\tau_{ac}}{\tau_{ab}} = \begin{pmatrix} 3/2 & 1 & 1/2 \\ +1/2 & 0 & -1/2 \end{pmatrix}^2 \begin{pmatrix} 3/2 & 1 & 1/2 \\ +1/2 & -1 & 1/2 \end{pmatrix}^{-2} = 2. \tag{17}$$

This relation is true for any substate M_I of the $^2P_{3/2}$ excited state. Since[15]

$$\frac{1}{\tau_a} = \frac{1}{\tau_{ab}} + \frac{1}{\tau_{ac}} = \frac{1}{16 \text{ nsec}}, \tag{18}$$

we find $\tau_{ac} = 48$ nsec, and $\tau_{ab} = 24$ nsec, as shown in Fig. 10a. The dipole for the $|b\rangle$ to $|a\rangle$ transition can then be found from[16]

$$\frac{1}{\tau_{ab}} = \frac{4\omega_o^3 (p_{D_2})^2_{-1/2,3/2 \rightarrow -1/2,3/2}}{3\hbar c^3} \tag{19}$$

giving $(p_{D_2})_{-1/2,3/2 \rightarrow -1/2,3/2} = 5.1\times10^{-18}$ esu cm as the dipole moment for any allowed transition between sublevels of the $^2S_{1/2}$ ground state and sublevels of the $^2P_{3/2}$ excited state. This transition dipole moment is related to the McCall-Hahn dipole moment by[3,1]

$$(p_{D_2})^{M.H.}_{-1/2,3/2 \rightarrow -1/2,3/2} = \frac{(p_{D_2})_{-1/2,3/2 \rightarrow -1/2,3/2}}{\sqrt{2}} = 3.68\times10^{-18} \text{ esu-cm} \equiv \sqrt{2}p_o. \tag{20}$$

The intensity required for a 2π square pulse can now be calculated

$$\frac{2p}{\hbar}\int \mathcal{E}dt \simeq \frac{2p}{\hbar}\mathcal{E}_{max}\,\tau_p = 2\pi;\quad I = \frac{c\mathcal{E}_{max}^2}{4\pi} = \frac{c\pi\hbar^2}{4p^2\tau_p^2} = 7.7\ \text{W/cm}^2 \tag{21}$$

with $\tau_p = 5$ nsec.

In the same way, we can calculate the ratio of the partial lifetimes of the $^2P_{1/2}(M_J=-1/2, M_I=3/2)$ excited state giving

$$\frac{\tau_{ac}}{\tau_{ab}} = 1/2 \tag{22}$$

so that $\tau_{ac} = 24$ nsec and $\tau_{ab} = 48$ nsec as shown in Fig. 10b. The transition dipole moment for the $^2S_{1/2}$ to $^2P_{1/2}$ transition is then:

$$(p_{D_1})^{M.H.}_{-1/2,3/2\ \rightarrow\ -1/2,3/2} = \frac{(p_{D_2})^{M.H.}_{-1/2,3/2\ \rightarrow\ -1/2,3/2}}{\sqrt{2}} = p_o. \tag{23}$$

So that the intensity for a 2π pulse will be:

$$I = 7.7/\sqrt{2}\ \text{watts/cm}^2.$$

Experimentally this difference in transition dipole moment of the $^2S_{1/2}$ to $^2P_{3/2}$ transition and the transition dipole moment of the $^2S_{1/2}$ to $^2P_{1/2}$ transition was observed. For the same input pulse, the output pulse on the D_1 transition exhibited characteristic 4π breakup while 6π breakup was seen on the D_2 transition (compare Fig. 11a and 11b).

For light circularly polarized along the magnetic field the allowed transitions correspond to $\Delta M_J = \pm 1$. As in the previous cases the transition dipole moment of the allowed transitions can be found from the lifetime of the excited state. For the D_1 transition the $^2P_{1/2}$ ($M_J=1/2, M_I=3/2$) state $|a\rangle$ can make a transition to the $^2S_{1/2}$ ($M_J=-1/2, M_I=3/2$) state $|b\rangle$ or the $^2S_{1/2}$ $M_J=+1/2$, $M_I=3/2$) state $|c\rangle$. The ratio of the partial lifetimes of the excited state is then given by[14]

$$\frac{\tau_{ac}}{\tau_{ab}} = \begin{pmatrix} 1/2 & 1 & 1/2 \\ -1/2 & 1 & -1/2 \end{pmatrix}^2 \begin{pmatrix} 1/2 & 1 & 1/2 \\ -1/2 & 0 & 1/2 \end{pmatrix}^{-2} = 2 \tag{24}$$

which gives by Eq. (18),

$$\tau_{ac} = 48 \text{ nsec and } \tau_{ab} = 24 \text{ nsec.}$$

This decay scheme is shown in Fig. 10c. Since it is exactly the same as the decay scheme for linearly polarized light on the D_2 transition the transition dipole moment between states $|a\rangle$ and $|b\rangle$ is also the same and found from Eq. (19) to be

$$(p_{D_1})^{M.H.}_{1/2,3/2 \rightarrow -1/2,3/2} = \sqrt{2}p_o. \tag{25}$$

Likewise we can calculate the ratio of partial lifetimes of the $^2P_{3/2}$ ($M_J=1/2, M_I=3/2$) excited state giving

$$\frac{\tau_{ac}}{\tau_{ab}} = 1/2, \tag{26}$$

so that $\tau_{ac} = 24$ nsec and $\tau_{ab} = 48$ nsec as shown in Fig. 10d. The dipole moment for this transition then is

$$(p_{D_2})^{M.H.}_{1/2,3/2 \rightarrow 3/2,3/2} = p_o. \tag{27}$$

For the $^2P_{3/2}$ ($M_J=3/2, M_I=3/2$) excited state, decay can only occur to the $^2S_{1/2}$ ($M_J=1/2, M_I=3/2$) state. This transition is therefore a two level system and τ_{ab} is just the total lifetime 16 nsec. It is interesting to point out that in this case coherent optic studies can be made on a pure two level system, that is, there is no complication of a third level. The transition dipole moment can be found by comparison with the D_1 transition dipole previously considered. Since the lifetime for the $|a\rangle$ to $|b\rangle$ transition in that case was 48 nsec the dipole moment in this case will be $\sqrt{3}$ larger and equal to

$$(p_{D_2})^{M.H.}_{1/2,3/2 \rightarrow 3/2,3/2} = \sqrt{3}p_o. \tag{28}$$

Experimentally these differences in transition dipoles moments were also observed. For the same input pulse, the output pulse on the D_1 transition exhibited characteristic 4π breakup while the $^2S_{1/2}$ ($M_J=-1/2$) to $^2P_{3/2}$ ($M_J=+1/2$) D_2 transition exhibited 3π characteristics and the $^2S_{1/2}$ ($M_J=+1/2$) to $^2P_{3/2}$ ($M_J=3/2$) D_2 transition exhibited characteristic 6π breakup (Fig. 12).

C. Weak Magnetic Field

In a weak magnetic field the good quantum numbers are I, J, F, M_F. In this case, the dipole moment for a transition between a given $|FM_F\rangle$ ground state to a $|F'M_F'\rangle$ excited state will be different for different $|F'M_F'\rangle$. In order to analyze SIT data it therefore becomes necessary to calculate the dipole moment for each degenerate transition. Since we are only interested in the relative dipole moments we choose, as a convenience, the dipole moment of the $^2S_{1/2}$ to $^2P_{1/2}$ transition with linearly polarized light in high magnetic fields as a reference.

For simplicity we consider first the D_1 transition. For light linearly polarized parallel to the magnetic field and the wave vector perpendicular to the magnetic field the allowed transitions are shown in Fig. 13. It is important to point out that in taking the good quantum numbers to be F and M_F we have assumed that the hyperfine interaction is stronger than the interaction between the electromagnetic field of the optical pulse and the dipole moment of the atom. That is,

$$p \cdot E < h\Delta\nu_{HF}. \tag{29}$$

For a $2\pi n$ pulse we can estimate $p \cdot E$ as

$$\frac{2p\mathcal{E}_{max}\tau_p}{\hbar} = 2\pi n$$

$$p\mathcal{E}_{max} = \frac{2\pi\hbar n}{2\tau_p} = \frac{hn}{2\tau_p} \approx nh\Delta f, \tag{30}$$

where Δf is the Fourier transform of our pulse and is 60 MHz. For a 4π pulse

$$p \cdot E/h = 120 \text{ MHz}. \tag{31}$$

Since the hyperfine interaction energy for the $^2P_{1/2}$ state is 192 MHz, the condition $p \cdot E < h\Delta\nu_{HF}$ is assumed valid and each allowed transition may be considered distinct. The relative dipole strengths can then be calculated by

$$p^2 = C\,|\langle F'M_F'|r_0^1|FM_F\rangle|^2$$

$$p^2 = C\begin{pmatrix} F' & 1 & F \\ -M_F' & 0 & M_F \end{pmatrix}^2 (2F+1)(2F'+1) \tag{32}$$

$$X\begin{Bmatrix} J' & F' & I \\ F & J & 1 \end{Bmatrix}^2 (J'\|r\|J)^2.$$

These values are then compared with the dipole moment of the D_1 transition with linearly polarized light in a large magnetic field which is given by

$$(p_{D_1})^2_{L.P.} = C|\langle J'M_J'I'M_I'|r_0^1|JM_JIM_I\rangle|^2$$

$$= C\begin{pmatrix} J' & 1 & J \\ -M_J' & 0 & M_J \end{pmatrix}^2 (J'\|r\|J)^2 = p_o^2. \tag{33}$$

Since we are interested in the relative values of the dipole moments we assign $p_o = 1$. The results are tabulated

in Table 1. These results remain valid even as the magnetic field is lowered to zero since the excited transitions remain distinct due to the large hyperfine separation. Therefore, for weak magnetic fields on the order of 0 to 150 Gauss, several different but clearly defined transition dipoles are excited by the optical pulse (Table 1). Experimental results for this case (Fig. 14a,15a,16a,17) indicate that the features of SIT are sharp and, in fact, do not differ very much from the high field nondegenerate case.

For the D_2 transition the condition

$$p \cdot E < h\Delta\nu_{HF} \tag{34}$$

is not satisfied. The hyperfine splitting of the $^2P_{3/2}$ excited state varies between 19 and 60 MHz as discussed in Sec. III-A. Therefore,

$$p \cdot E > h\Delta\nu_{HF} \tag{35}$$

is assumed to be valid in this case. A weak magnetic field of 60 to 150 Gauss is large enough to decouple I and J for the excited state so that the good quantum numbers are J, M_J, I, M_I for the excited state. The ground state hyperfine splitting energy is large, however, so that for fields between 60 and about 150 Gauss the good quantum numbers are I,J,F,M_F for the ground state.

From the equation

$$\frac{\Delta W}{h} = \frac{\mu_0 H_0}{h} [g_J(^2P_{3/2})] = 1.67 \text{ MHz/Gauss} \tag{36}$$

the separation between the $M_J = 1/2$ and $M_J = -1/2$ substates of the $^2P_{3/2}$ excited state is on the order of 110 to 220 MHz. Therefore, transitions between the $^2S_{1/2}$ ground states to the $^2P_{3/2}$ ($M_J=1/2$) excited states can be considered distinct from transitions to the $^2P_{3/2}$ ($M_J=-1/2$) excited states. These transitions are shown in Fig. 18. The relative dipole strengths can then be calculated by

$$p^2 = C|\langle J' M_J' I \; M_I' | r_0^1 | F M_F I J \rangle|^2$$

$$= C \begin{pmatrix} J' & 1 & J \\ -M_J' & 0 & M_J' \end{pmatrix}^2 \begin{pmatrix} J & I & F \\ M_J' & M_I' & -M_F \end{pmatrix} \qquad (37)$$

$$\times (2F+1)(J' \| r \| J)^2.$$

These values are compared with the dipole moment of the D_1 transition for linearly polarized light in a large magnetic field and the relative values are tabulated in Table 2.

Therefore, for fields between 60 and 150 Guass, several different but clearly defined dipoles (Table 2) are excited by the optical pulse. Experimental results show (Fig. 19a and 20a), in this case, that although the features of SIT are diminished all of the characteristics of SIT, including pulse breakup, are to some degree observed.

As the magnetic field is lowered the transitions between the $^2S_{1/2}$ ground states and the $^2P_{3/2}$ ($M_J=1/2$) excited states are no longer distinct from transitions to the $^2P_{3/2}$ ($M_J=-1/2$) excited states. The allowed transitions are shown in Fig. 21b. However, a representation may be chosen

in which all transitions are distinct and have identical transition dipole moments.[7] Therefore, nondegenerate self-induced transparency should be observed and the characteristics of SIT should be as sharp as in the high magnetic field case. Experimental results were in complete agreement with this theoretical prediction (Fig. 21a). That a representation can be chosen in which all transitions are distinct and have the same transition dipole moment is shown in the following analysis. As shown in Fig. 18, each sublevel of the $^2S_{1/2}$ ground state is now excited to two excited states. For example, the $^2S_{1/2}$ $(F=1, M_F=-1)$ state $|b\rangle$ is excited to the $^2P_{3/2}$ $(M_J=1/2, M_I=-3/2)$ state $|a\rangle$ and to the $^2P_{3/2}$ $(M_J=-1/2, M_I=-1/2)$ state $|d\rangle$. The basis for the excited state of the atom is now transformed from $|a\rangle$ and $|d\rangle$ to ψ_1 and ψ_2. Where

$$\psi_1 = \frac{p_a}{(p_a^2+p_b^2)^{1/2}}|a\rangle + \frac{p_b}{(p_a^2+p_b^2)^{1/2}}|b\rangle$$

and (38)

$$\psi_2 = \frac{p_a}{(p_a^2+p_b^2)^{1/2}}|b\rangle - \frac{p_b}{(p_a^2+p_b^2)^{1/2}}|a\rangle$$

The coefficients were chosen to satisfy the conditions

$$\psi_1^* \psi_1 = \psi_2^* \psi_2 = 1$$

$$\psi_1^* \psi_2 = 0$$

$$|\langle \psi_1 | r | c \rangle|^2 = p_a^2 + p_b^2 \tag{39}$$

$$\langle \psi_2 | r | c \rangle = 0$$

Therefore, with ψ_1 and ψ_2 as the wavefunctions for the excited states there is only one transition dipole moment given by

$$p = \langle \psi_1 | r | c \rangle = \sqrt{p_a^2 + p_b^2} \tag{40}$$

The same procedure may be followed for all sublevels of the $^2S_{1/2}$ (F=1) ground state and $^2S_{1/2}$ (F=2) ground state giving the result that all transition dipoles are independent, identical, and have the value $p = \sqrt{2}$ relative to the D_1 transition dipole moment for linearly polarized light in a large magnetic field.

Footnotes

10. N. F. Ramsey, Molecular Beams (Oxford U.P., Oxford, England, 1956), p. 74.

11. T. W. Hansch, I. S. Shahin, A. L. Schawlow, Phys. Rev. Lett. 27, 707 (1971).

12. F. Schuda, M. Hercher, and C. R. Stroud, Jr., Appl. Phys. Lett. 22, 360 (1973).

13. A. C. G. Mitchell and M. W. Zemansky, Resonance Radiation and Excited Atoms (Cambridge at the University Press, N.Y., N.Y., 1961), p. 99 Eq. (33)

14. A. R. Edmonds, Angular Momentum in Quantum Mechanics (Princeton U.P., Princeton, N.J., 1957).

15. R. J. Wolf and S. P. Davis, J.O.S.A. 58, 490 (1968).

16. L. I. Schiff, Quantum Mechanics, 2nd ed. (McGraw-Hill, New York, 1955), p. 253, Eq. (35.21).

IV. Pulse-Area-Pulse-Energy Approach

In the McCall-Hahn theory[1] of self-induced transparency, Bloch's equations and Maxwell's equations are solved simultaneously to yield a self consistent solution which describes the evolution of the pulse. For the experiment in Na, as in a previous experiment in Rb,[3] Bloch's equations must be modified to correctly include spontaneous decay effects to a third level. The modified Bloch equations and Maxwell's equations could then be used to simulate our experiment on a computer and a comparison could be made between theory and experiment. In Rb such a comparison was made and excellent agreement found.[3] Since the Na experimental results in a large magnetic field (Fig. 11) are nearly identical to the Rb results taken under similar conditions, there is good agreement between theory and experiment in the Na case also.[17]

In a weak magnetic field, however, there exists no previous detailed experiment with which to compare, and direct comparison between theory and experiment becomes important if any conclusions about degeneracy effects are to be made. However, we are not interested in a detailed analysis of SIT in Na with degeneracy. Rather, it would be more valuable to compare experiment with theory in a simple way in order to understand the effect of degeneracy

on the SIT effect. In this way one may be able to make general statements on degeneracy effects which would be applicable to other systems as well as the experiment in Na. This goal can be achieved by comparing the experiment with the pulse-area-pulse-energy approach by McCall and Hahn.[7]

For a simple two-level system the area theorem[1,7] can be written as

$$\frac{dA}{dz} = -\frac{\alpha}{2} S(A) \tag{41}$$

where $S(A) = \sin A$ and $A \equiv \frac{2p}{\hbar} \int_{-\infty}^{\infty} \mathcal{E}(z,t)dt$. This theorem, which is derived from Maxwell's and Bloch's equations, describes the evolution of the area of the pulse. In the same way the equation[1,7]

$$\frac{d\mathcal{J}}{dz} = -\alpha \mathcal{J} F(A,\mathcal{J}, \text{ pulse shape}), \tag{42}$$

where $\mathcal{J} \equiv \frac{c}{4\pi} \int_{-\infty}^{\infty} \mathcal{E}^2(z,t)dt$ is the pulse energy per unit area, describes the evolution of the energy of the pulse. The quantity F describes deviations from Beer's Law and gives quantitative information about losses in the system. It has been shown that F(A) can be estimated by[7]

$$F(A) = \frac{2(1-\cos(A))}{A^2} . \tag{43}$$

Together these two equations, in a simplified and qualitative way, provide a method to analyze the effect of degeneracy on SIT phenomena.

When degeneracies are present, the area theorem can be generalized to[1,7]

$$\frac{dA}{dz} = -\frac{\alpha}{2} S(A) = -\frac{\alpha}{2} \frac{\sum_i g_i p_i \sin(p_i A)}{\sum_i g_i p_i^2} \tag{44}$$

where, as discussed in Sec. III-C, p_i are the relative transition dipole moments taken with respect to the linearly polarized transition dipole moment of the D_1 transition in Na which was assigned the value 1. A is always defined as the area for the dipole of value 1, i.e.

$$A \equiv \frac{2(1)}{\hbar} \int \mathcal{E} dt, \tag{45}$$

and g_i are the statistical weights for the degenerate p_i excited dipoles.

Likewise the equation describing the energy of the pulse can be generalized[1,7] to

$$\frac{d\mathcal{J}}{dz} = -\alpha \mathcal{J} F(A) \tag{46}$$

$$\text{where } F(A) = \frac{\Sigma g_i p_i^2 \, 2(1-\cos(p_i A))/(p_i^2 A^2)}{\Sigma g_i p_i^2} . \tag{47}$$

In addition to the pulse area and pulse energy, an interesting and useful quantity to consider is the evolution of the energy stored in exactly resonant atoms which is given by

$$W(A) \propto \frac{\Sigma g_i \, 2(1-\cos(p_i A))}{\Sigma g_i} . \tag{48}$$

In Fig. 22 we plot S(A) and W(A) as a function of area for the case of a single excited dipole, such as, the D_1 or D_2 line for Na in large magnetic fields. These curves do not describe the evolution to a hyperbolic secant traveling-wave pulse. Detailed information about the shape, width, or peak intensity of the pulse is beyond the capability of the Energy-Area equations. However, much can be learned about the general features of the SIT effect. Features, such as, stable areas, losses, propagation and pulse widths, can be quantitatively estimated by the pulse-area-pulse-energy equations or the curves of Fig. 22 . In addition, features, such as, peak amplification and pulse breakup can be qualitatively described by the theory. For example, (Fig. 22) stable areas of multiples of 2π (or less than 2π if losses are included) are quantitatively predicted by the S(A) curve. W(A) and F(A) indicate that a stable area is accompanied by lossless propagation. If the input pulse area is slightly above π, S(A) indicates that the pulse area will evolve to 2π while W(A) and F(A) indicate that during the evolution to a 2π area pulse, energy will be lost and the atoms left excited. Together these curves indicate that the pulse width will have to increase to achieve an area of 2π. W(A) also indicates that the 2π stable area solution can be described as energy being absorbed during the first half of the pulse, when energy stored in the atoms is increasing, followed by energy being returned to the

pulse during the second half of the pulse, when stored energy in the atoms is decreasing.

For an input area slightly less than 3π, W(A) indicates that energy is absorbed during the first third of the pulse, returned to the peak of the pulse during the second third and absorbed during the final third. As a result, peaking and narrowing of the input pulse is expected during evolution to a stable 2π area. For an input area near 4π, S(A) indicates that the pulse evolves to a stable 4π area. W(A) describes the evolution as energy being absorbed during the first quarter of the pulse, returned during the second quarter while peaking above the input pulse, absorbed during the third quarter while dipping below the input pulse, and returned during the final quarter while again peaking above the input pulse. As a result pulse breakup features can be qualitatively explained in this way.

Footnotes

17. For the Na experiment, the optical pulse shape was very nearly identical to the Rb experiment since the same Pockels cell was used. The only theoretical difference between the two experiments was the values of T_1 and T_2'. However, computer analysis of the Rb experiment indicated that results were not sensitive to T_1 and T_2' as long as they were a few times larger than τ_p. For Na this is the case.

V. Comparison Between Theory and Experiment

The pulse-area-pulse-energy analysis will now be applied to the case where several dipoles, which differ in magnitude, are excited by an optical pulse. In our analysis, emphasis will be placed on pulse breakup since experimentally, it was this feature of the SIT effect which seemed the most sensitive to degeneracy effects.

For example, in all cases, propagation with very little loss was seen to occur. In fact, the predicted loss by the function F(A) was on the order of relaxation losses due to finite T_1 and T_2'. Therefore, measuring energy loss for a stable area did not seem to be a sensitive approach. Comparison of the value of stable pulse areas which evolve would seem a difficult approach since it requires accurate determination of the area of the pulse. Pulse delay times are also highly dependent on losses in the system which again do not deviate substantially from the loss due to finite T_2' and T_1. On the other hand, pulse breakup could be quickly observed and qualitatively compared.

A. Weak Field D_1 Transitions

For the data of Fig. 14a the dye laser was tuned (900 MHz off center) to the low frequency side of the D_1

transition in a weak magnetic field. For light linearly polarized parallel to the field, this corresponds to transitions between M_F sublevels of the $^2S_{1/2}$ (F=2) ground state to M_F sublevels of the $^2P_{1/2}$ excited state (Fig. 14b). The data indicate that although several transition dipoles are excited, the characteristics of SIT phenomena are nearly as clear as in the nondegenerate case. In particular, pulse breakup is clearly present. The function S(A) is plotted in Fig. 14c. This curve indicates that stable areas do exist at values near 2π and 4π. The F(A) curve (Fig. 14e) indicates that nearly lossless propagation will occur after evolution to a stable area. W(A), plotted in Fig. 14d indicates that energy is absorbed and returned to the pulse in much the same way as in the nondegenerate case (Fig. 22). For this reason, it may be theoretically argued that features, such as pulse breakup and peaking, should be as clear in this degenerate case as in the nondegenerate case. This may even be more nearly true experimentally since the detector resolution was about 1nsec. Physically, the predicted results can be understood by examining the relative value of the various transition dipoles. There are three distinct dipoles which have the relative values 1, $\sqrt{3/4}$, $\sqrt{1/4}$. They also differ in statistical weight as seen in Table 1. Since the two largest transition dipoles are not very different (.86 to 1) and since the largest transition dipole is dominant in intensity (absorption 2 to 1), it is not surprising that the two dipole types are radiating and absorbing energy

together during the time of the pulse. It is also reasonable that the stable area is slightly greater than 4π for the largest transition dipole and a little under 4π for the weaker transition dipole in an effort to minimize losses by satisfying the excited dipoles with a pulse as close as possible to 4π in area for both. The smallest transition dipole (1/2) is small in area and low in intensity (3 to 1) compared to the largest transition dipole. As a result it does not affect the change in energy in the atoms during the absorption or emission stages of the evolution of the system. The fact that this transition dipole is exactly a factor of two lower in area than the largest transition dipole means that a 4π pulse for the larger transition dipole is a 2π pulse for the smallest giving low loss for both dipoles for the stable area near 4π.

The data shown in Fig. 15a were taken after tuning the laser to the center of the absorption profile, so that transition dipoles are excited from both the F=1 and F=2 ground states (Fig. 15b). As a result, the largest transition dipole is not as dominant in intensity (absorption 4 to 3), and we can expect smaller changes in the energy stored in the atoms as indicated in the W(A) curve in Fig. 15d. However, an area of slightly above 4π for the largest transition dipole and slightly below 4π for the weaker transition dipole still corresponds to low-loss propagation as seen in the S(A) curve (Fig. 15c) and the F(A) curve (Fig. 15e). Qualitatively then, we may expect some small changes in SIT characteristics,

especially breakup, as was the case (compare Fig. 15a to Fig. 14a).

As the laser was tuned from the center to the high-frequency side of the D_1 line, we noticed two things. First, pulse breakup features were diminishing and second, α was decreasing. The decrease in the absorption coefficient is easily explained since α on the high-frequency side is lower by a factor of $\frac{3}{5}$ from α on the low-frequency side. The allowed transitions are shown in Fig. 16b. Furthermore, the statistical weights now make the largest dipole moment weaker in intensity than the intermediate dipole (absorption 2 to 3) and closer to the intensity of the lowest dipole (absorption 2 to 1). As a result pulse breakup is expected to diminish as seen experimentally when tuned 900 MHz off center (Fig. 16a). The S(A) and F(A) curves (Fig. 16c and 16e) are little changed from similar curves on the low frequency side (Fig. 14). The W(A) curve (Fig. 16d) indicates that smaller changes in the energy stored in the atoms can be expected resulting in poorer pulse breakup. However, since α has also diminished, it is possible that the poorer feature of pulse breakup could be due to the change in αL for the sample. In Fig. 17 we have increased αL in order to answer this question and find that pulse breakup features improve. In fact, although they do not seem to be as good as breakup features on the low-frequency side, they do not differ substantially.

In summary SIT characteristics on the D_1 transition in weak magnetic fields are not very different from the nondegenerate case in large magnetic fields. In addition, the characteristics of SIT do not vary much as we tune the laser from the low frequency side of the D_1 transition (F=2) to the high frequency side (F=1). This agrees well with theory since the S(A), F(A), and W(A) curves are not very different from the nondegenerate case and do not vary much from the low frequency side to the high frequency side of the D_1 transition.

B. D_2 Transitions: High Field for the Excited State Low Field for the Ground State

For the data of Fig. 19a the dye laser was tuned (900 MHz off center) to the high-frequency side of the D_2 transition (F=1) in a field of 60 to 150 Gauss. The allowed transitions for light linearly polarized parallel to the magnetic field are shown in Fig. 19b. As discussed in Sec. III-C all transitions can be considered distinct. The data show that pulse breakup is not as sharply defined as in the previous case for the D_1 transition (compare Fig. 19a with Fig. 14a). The function S(A) is plotted in Fig. 19c. This curve indicates that a stable area does exist near 2π but there is some doubt about a 3.2π stable area. The addition of losses could make the stable area unstable. The F(A) curve (Fig. 19e) indicates that stable areas are accompanied by higher losses than in the D_1 case (compare

Fig. 19e with Fig. 14e). The W(A) curve (Fig. 19d) indicates that the change in energy in the atoms as a function of area is not as large as in the case of the D_1 transition (compare Fig. 19d with Fig. 14d). Energy absorbed from the pulse during the first quarter is nearly the same as in the D_1 line case. Energy returned to the pulse during the second quarter is less than in the D_1-line case so that peaking of the first peak is expected to be less. During the third quarter less energy is absorbed than in the D_1 case and therefore the valley in the output pulse is expected to be less. For the last quarter considerably less energy is returned to the pulse so that the second peak is expected to be much lower in the D_2 case than the D_1 case. Over all, pulse breakup on the high frequency D_2 transition is expected to be poorer than the D_1 transition. Experimentally, this was clearly the case.

As the laser was tuned from the high-frequency side of the line to the low, the absorption increased (as expected since α increases by a factor of 5/3) and pulse breakup became slightly less pronounced. The allowed low frequency D_2 transitions are shown in Fig. 20b. S(A) and F(A) curves look very much alike (compare Fig. 20c,e and 19c,e) for either side of the line. W(A), however, does indicate that energy absorbed or returned to the field is less for the low frequency side than high frequency side. This indicates that pulse breakup features would be diminished on the low frequency side of the resonance as was observed experimentally.

The observed difference (1800 MHz off center) however, was small (compare Fig. 20a with Fig. 19a).

In summary, SIT characteristics of pulse breakup were experimentally observed to be considerably poorer for the D_2 transition than the D_1 transition. Comparison of W(A), S(A), and F(A) curves for both transitions also indicate relatively less pronounced breakup for the D_2 transition. However, in all cases, the characteristic features of nonlinear transmission and long delays remained similar to nondegenerate SIT.

Physically, why does one see poorer breakup on the D_2 transition? The answer is that the dipoles compete more in the case of the D_2 transitions. For the D_1 transition the relative dipoles are 1, 0.87, and 0.5. The stable area of 4.2π then corresponds to an area of 3.7π for the .87 dipole and 2.1π for the 0.5 dipole. Therefore, the pulse has chosen the "best" area to, as efficiently as possible, return the excited atoms back to the ground state. However, in the D_2 high-frequency case the excited dipoles are 1.22, 1.0, 0.7. A stable area of 3.2π for the intermediate transition dipole of relative magnitude 1, corresponds to 3.94π and 2.24π for the 1.22 and 0.7 transition dipoles respectively. Therefore, the stable area of 3.2π almost returns the 0.7 and 1.22 transition dipoles to the ground state but leaves the intermediate transition dipole excited. This accounts for the higher value of F(A) at the stable area for the D_2 case (Fig. 19e) as compared to the value of F(A) at the stable area for the

D_1 case (Fig. 14e). Interrelated with the higher value of F(A) is the fact that these three transition dipole types are not radiating and absorbing energy from the pulse at the same time. For example, during the time of the pulse which corresponds to an area changing from 2π to 3π for the 1.22 transition dipoles energy is being absorbed from the pulse and stored in the atoms. However, an area change from 2π to 3π for the 1.22 transition dipoles correspond to an area change of 1.16π to 1.74π for the .7 transition dipoles and 1.64π to 2.46π for the 1.0 transition dipoles. This means that these dipole types do not work together as they do in the case of the D_1 transition, to modulate the optical pulse. Rather, while one transition dipole type (1.22) is absorbing energy from the pulse, the second (.7) is returning energy to the pulse, and the third (1.0) does both. As a result, the energy (W(A)) stored in the atoms does not oscillate as much and pulse breakup characteristics are not as sharp. The same type of argument will apply for the low-frequency side of the D_2 transition where there are four different dipole types.

VI. Conclusions

The effects of degeneracy on SIT have been investigated by several authors.[7,18,19,20,21,22,23,24] All of the experimental work[18,21,24] and most of the theoretical work[20,21,22,23] have been directed toward gaseous SF_6 as the absorbing medium. These investigations were limited by the complicated degenerate system of SF_6. In fact, the question of the effect of degeneracy in SF_6 still remains the subject of debate today.[24]

In order to gain further insight on the effect of degeneracy and the limitations it imposes on SIT phenomena we have studied SIT in Na vapor using a dye laser. There are three advantages of the dye laser-Na system as compared to the CO_2 laser-SF_6 system. First, Na is a simpler system which has clearly defined degenerate transitions with known transition dipole moments. Second, there are at least two sets of clearly defined combinations of excited transition dipoles which can be studied independently. Third, in high magnetic fields the Na system becomes nondegenerate. Therefore, observation of SIT in the nondegenerate case can be directly compared with a system in which the only change is to make it degenerate.

The results of this investigation are as follows. On the D_1 transition there are three distinct excited transition

dipoles. Two are nearly equal and the third comparatively small. It was found in agreement with a pulse-area-pulse-energy analysis that SIT characteristics were not very different from the nondegenerate case. There are two conclusions which can be made. First, if the dipoles are nearly equal, SIT characteristics will not be appreciably affected. Second, if there is a dominant dipole, SIT will again not be appreciably affected.

On the D_2 transition there are again at least three distinct transition dipole moments. However, in this case there is no single dominant transition dipole moment. Rather, the difference in two of the transition dipole moments results in one absorbing energy from the pulse while the other reradiating energy to the pulse. As a result the transition dipoles do not work together to modulate the pulse. In this case, it was found that SIT characteristics were less pronounced than in the nondegenerate case. This result was qualitatively predicted by the pulse-area-pulse-energy analysis. There are two conclusions which can be made. First, if the transition dipole moments differ by an amount which prevents them from absorbing and reradiating energy simultaneously, pulse breakup characteristics, although present, will be largely diminished. Second, energy will be lost in this case, since a 2π area pulse for one transition dipole will be about 3π in area for the second transition dipole and therefore leave atoms excited as the pulse propagates through the medium.

In summary, for the Na-dye laser experiment, the characteristic features of nonlinear transmission and long delays were found to be similar in the degenerate and nondegenerate cases. Moreover, the features of peaking and pulse breakup were found for the D_1 degenerate case to be similar to nondegenerate SIT. Only for the D_2 degenerate case were the features of peaking and pulse breakup largely reduced. However, even in this case, the experiment suggests that if it were not for the limitation on αL imposed by T_2', it would be possible to sharpen pulse breakup features by simply increasing αL. Therefore, the presence of degeneracy, in general, does not as severely limit the application of pulse breakup or peaking for useful devices as was originally indicated by studies in SF_6.

A pulse-area-pulse-energy analysis has been shown to be a qualitative indicator of the relative extent of peaking and pulse breakup to be expected in a degenerate system. This is particularly useful since a pulse-area-pulse-energy analysis may be performed on a small computer, such as a PDP-8, as was the case in this experiment. Such an analysis is simpler and inexpensive in comparison to computer solutions of Bloch's and Maxwell's equations.

In addition to degeneracy studies, the dye laser-Na experiment demonstrates for the first time that a C.W. dye laser can be used to study coherent optical effects. Sharp characteristics of pulse breakup, peak amplification, pulse delays, and nonlinear transmission have been observed in Na

vapor. Moreover, it has been shown that by tuning the laser from the D_1 to the D_2 transition in Na it is possible to observe the difference in the transition dipole moment by the use of the characteristics of SIT. This therefore illustrates the potential of SIT phenomena to measure relative, if not absolute, transition dipole strengths. Finally, it has been shown that for the D_2 transition in Na nondegenerate SIT (or similar coherent optical effects) can be studied without the necessity of a magnetic field.

Footnotes

18. C. K. N. Patel and R. E. Slusher, Phys. Rev. Lett. 19, 1019 (1967).

19. S. L. McCall and E. L. Hahn, in The Physics of Quantum Electronics, edited by S. F. Jacobs and J. B. Mandelbaum (Optical Sciences Center, The University of Arizona, Tucson, Ariz., 1968), pp. 65-99.

20. C. K. Rhodes, A. Szöke, and A. Javan, Phys. Rev. Lett. 21, 1151 (1968).

21. C. K. Rhodes and A. Szöke, Phys. Rev. 184, 25 (1969).

22. C. K. N. Patel, Phys. Rev. A 1, 979 (1970).

23. F. A. Hopf, C. K. Rhodes, and A. Szöke, Phys. Rev. B 1, 2833 (1970).

24. A. Zembrod and Th. Gruhl, Phys. Rev. Lett. 27, 287 (1971).

25. F. A. Hopf and C. K. Rhodes, Optics Communications 8, 88 (1973).

Fig. 1. Diagram of Basic Apparatus
L_1 is the lens to focus the laser beam into the Na cell; L_2 is the lens to image the uniform-plane-wave region onto the aperture; L_3 is the lens to focus into the detector; MAG is the magnetic coils producing a magnetic field B directed into the paper; A_3 is the aperture to select the uniform portion of the excitation region; GP is the Glans prism and PC the Pockels cell; L_4 is the lens to move the argon waist in the dye cell to the edge of the stability range and mode match argon and dye waists; F.P. 1 is the Fabry-Perot to monitor the spectral width of the single longitudinal mode; F.P. 2 is the Fabry-Perot with a larger free spectral range to monitor the spectral width of the laser before and after inserting etalons into the cavity; O_1 is the Osram Lamp which was not excited electrically but was heated by heater tape. The fluorescence from this lamp was observed while the laser was tuned onto the D_1 or D_2 lines of Na; O_2 is the Osram Lamp which was excited electrically and used as a reference for spectrometer (S) in order to distinguish the D_1 line from the D_2 line in Na; and S is the spectrometer used to tune the dye laser to the D_1 or D_2 transitions in Na. This spectrometer made it easy to distinguish the D_1 from the D_2 transition in Na.

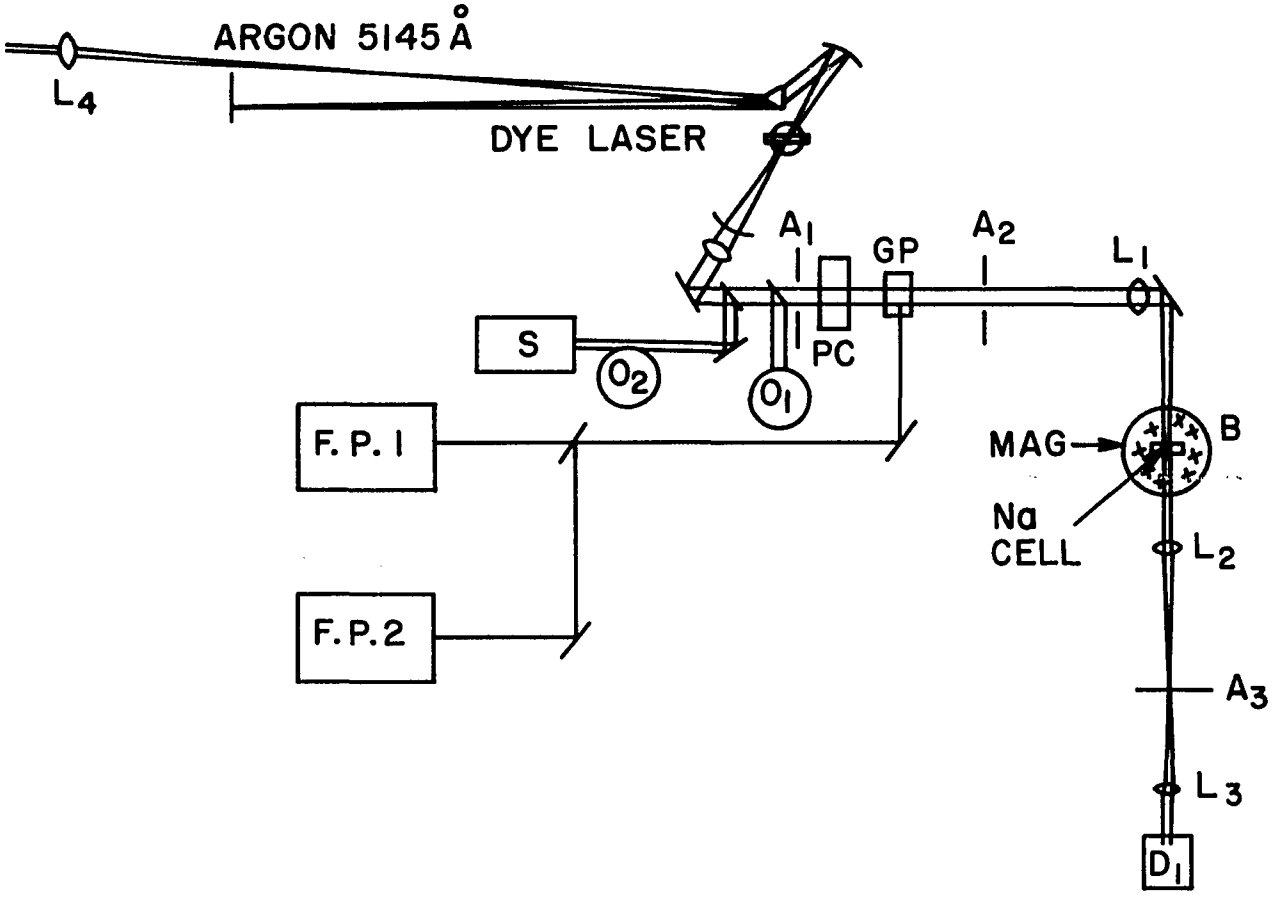
ARGON 5145 Å
L4
DYE LASER
A1
GP
A2
L1
S
PC
O2
O1
F. P. 1
F. P. 2
MAG
B
Na
CELL
L2
A3
L3
D1

FIG. 1

Fig. 2. Dye Laser Cavity
Argon pump beam is focused near mirror M_2 in order to move the argon waist in dye cell to same position as the dye laser waist when cavity is adjusted to edge of stability range. Dye cell and prism are at Brewster angle. Three etalons are used to narrow spectral output of laser to 20 MHz. On this edge of stability range the dye laser waist is focused on Mirror M_2.

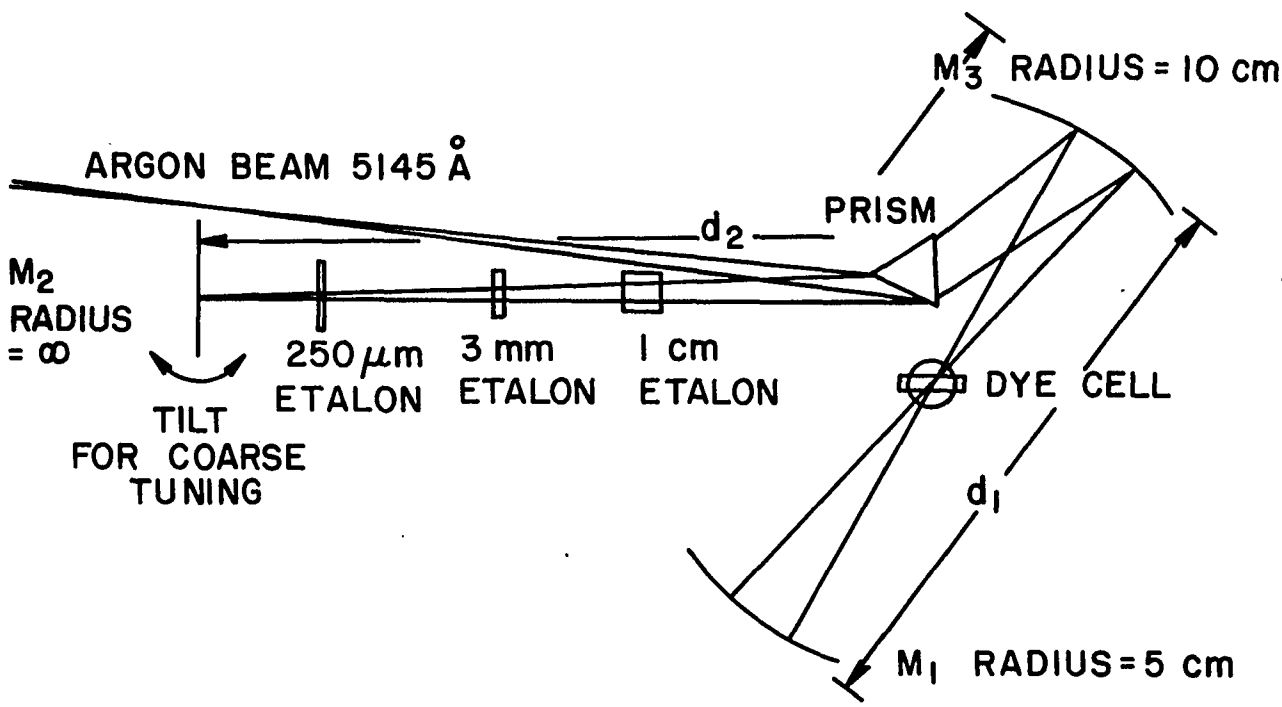
M3 RADIUS = 10 cm
ARGON BEAM 5145 Å
PRISM
d2
M2
RADIUS
= ∞
250 μm
ETALON
3 mm
ETALON
1 cm
ETALON
DYE CELL
TILT
FOR COARSE
TUNING
d1
M1 RADIUS = 5 cm

FIG. 2

Fig. 3(a). When dye laser cavity is adjusted near the edge of stability range where $d_1 = d_1(\max)$, the lowest order cavity mode is focused on M_2. The aperture prevents cavity modes which are parallel at M_2 from lasing (dotted lines). Shown in (b) is the dye laser cavity adjusted near other edge of stability range where $d_1 = d_1(\min)$. The lowest order mode is parallel at M_2. The aperture is not effective in preventing modes which are focused at M_2 from lasing (dotted lines).

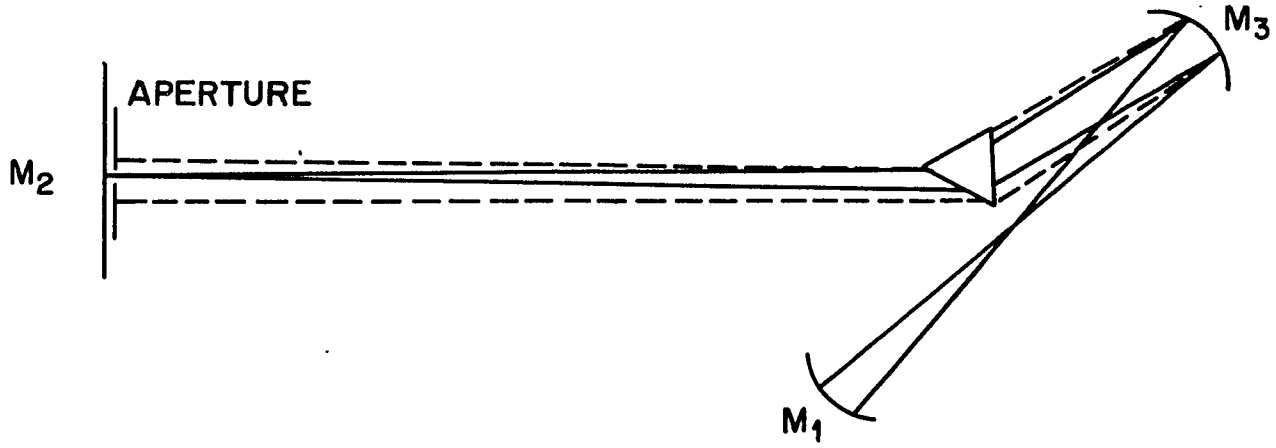

(a)

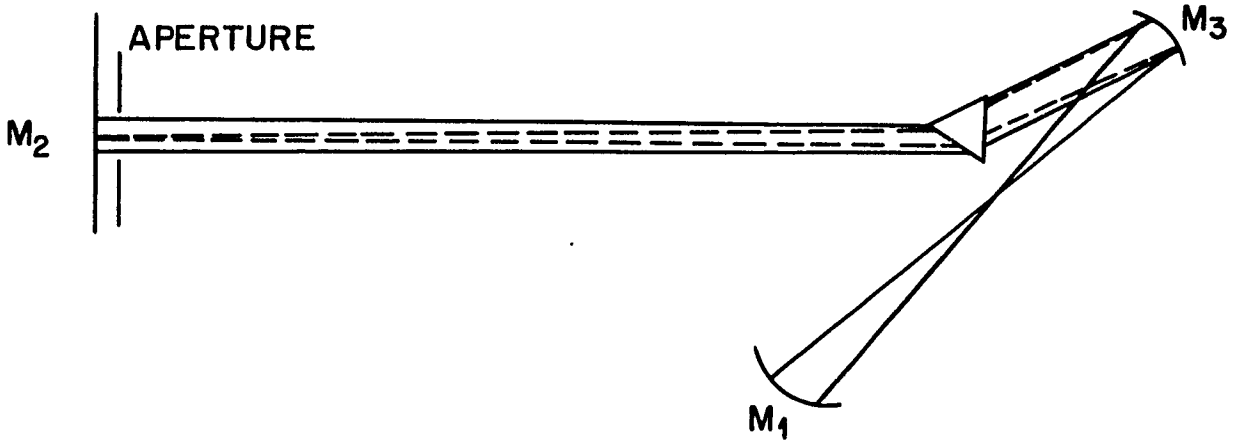

(b)

FIG. 3 (a AND b)

Fig. 4. Dye Circulating System
Dye is circulated by gear pump through a Millipore filter, buffer reservoir, and the dye cell. Dye velocity was about 18m/sec. A restriction at the output of the dye system was used to prevent cavitation.

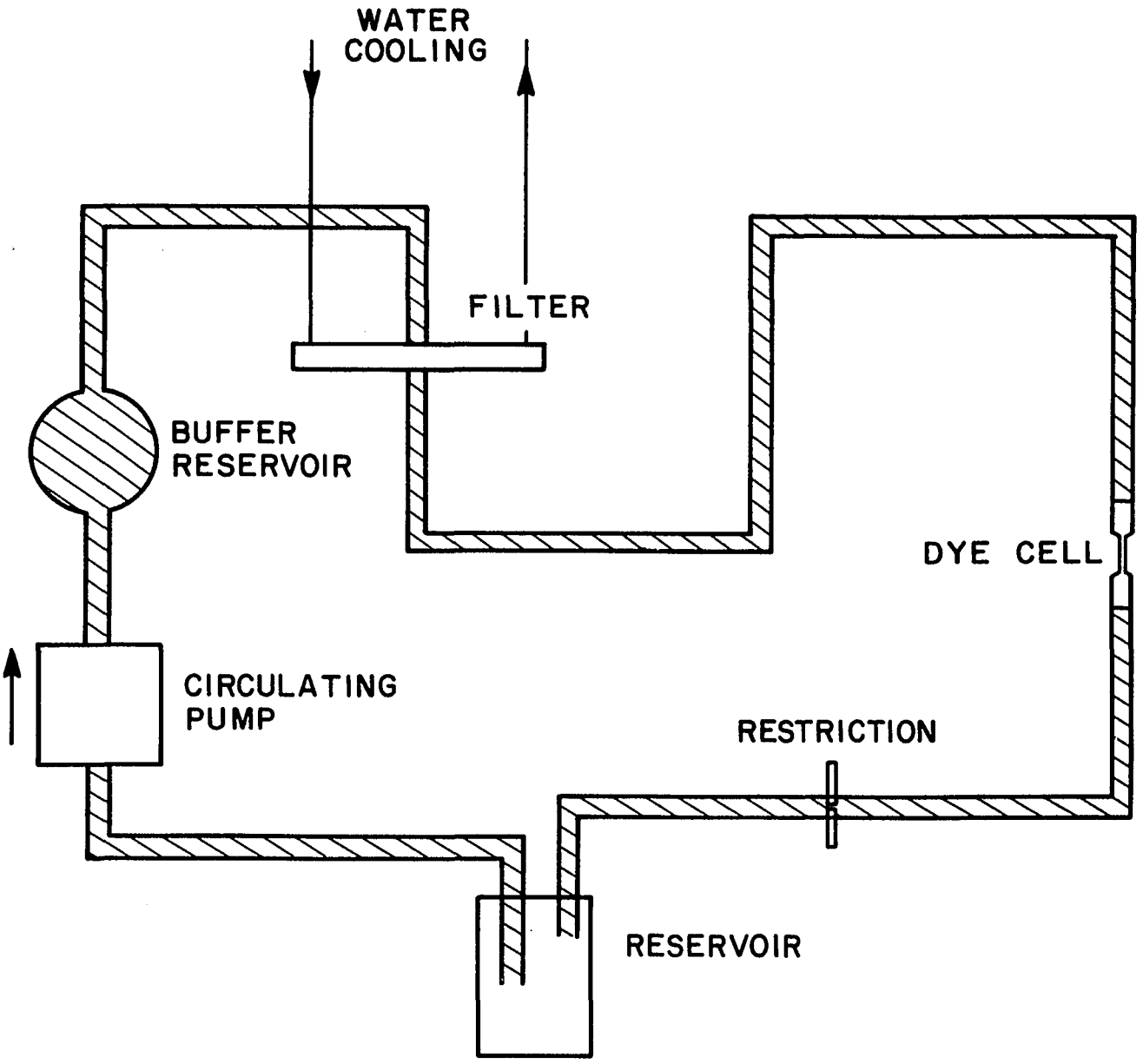
WATER
COOLING
FILTER
BUFFER
RESERVOIR
DYE CELL
CIRCULATING
PUMP
RESTRICTION
RESERVOIR

FIG. 4

Fig. 5. Dye Cells Used in Dye Laser
Cells A and B have a short flow path .64cm to allow a high dye velocity in the cell. No distinction was observed between cells A and B which were designed to give turbulent and laminar flow respectively. Cell C with the longer flow path 1.27cm gave rise to thermal problems.

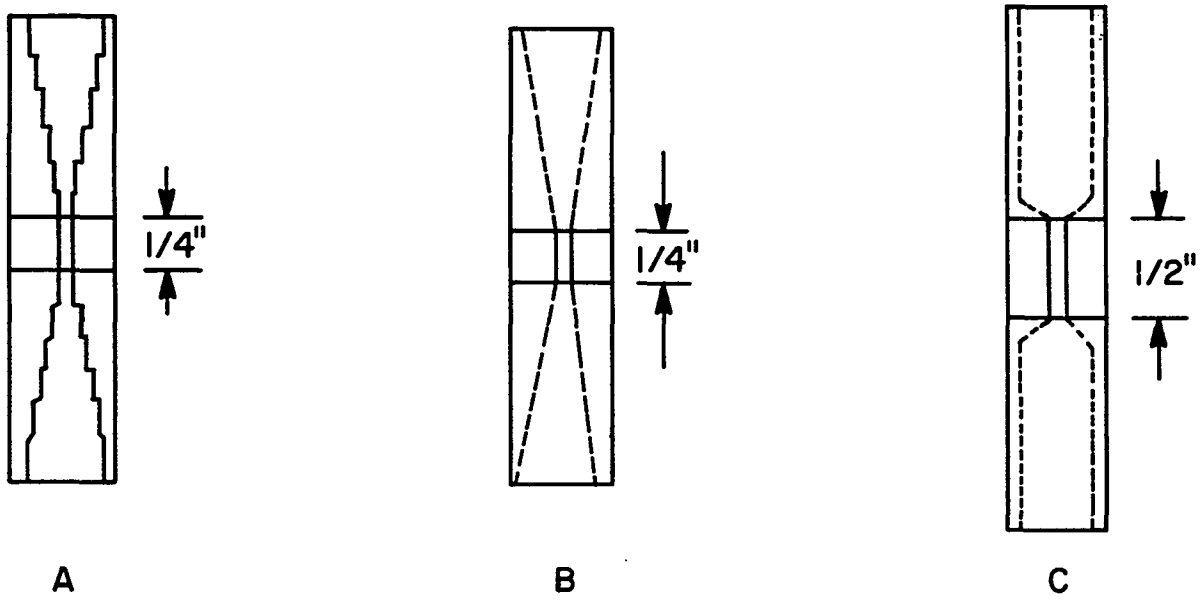

FIG. 5

Fig. 6. The reduction in spectral width due to each etalon. The spectral width with just the prism alone is about 40 GHz. The 250μm etalon narrows the spectral output to 25 GHz. Addition of the 3mm etalon reduces the profile to about 2.5 GHz. By adding the 1cm etalon operation in a single longitudinal mode is obtained. This mode is 20 MHz wide.

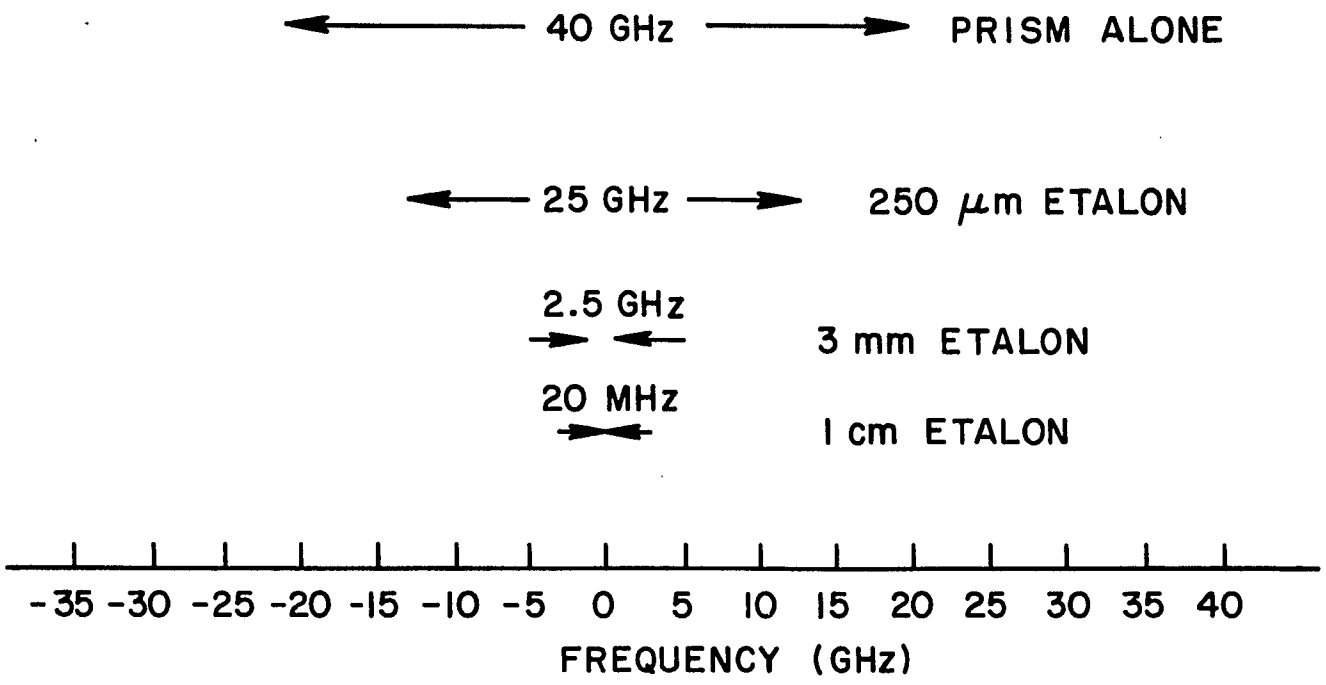
40 GHz
PRISM ALONE
25 GHz
250 μm ETALON
2.5 GHz
3 mm ETALON
20 MHz
1 cm ETALON
-35 -30 -25 -20 -15 -10 -5 0 5 10 15 20 25 30 35 40
FREQUENCY (GHz)

FIG. 6

Fig. 7. Uniform-Plane-Wave Condition
The excitation region of about 75μm was imaged by a 15.24cm lens onto a 100μm aperture. Since the image of the focal region was magnified by a factor of 3, the aperture selects the fraction of the excitation region which was nearly uniform in intensity for observation.

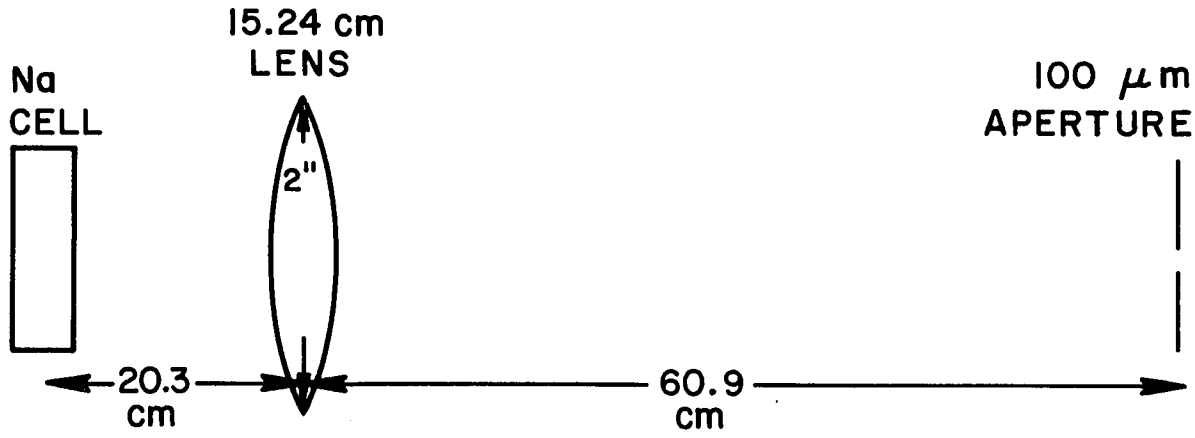

FIG. 7

Fig. 8. Energy level diagram of Na in a magnetic field not showing the zero-field hyperfine structure (see Fig. 9). In magnetic fields above 2 to 3 kG the good quantum numbers are J, M_J, I, M_I where, each M_J state has 4 M_I substates since $I = 3/2$. In this case the separation between M_I sublevels of the $^2P_{3/2}$ state is of the order of 25 MHz. For the $^2P_{1/2}$ state the separation is 48 MHz, and for the $^2S_{1/2}$ state 443 MHz. Since the Doppler width is 1700 MHz, transitions between M_I substates of the $|JM_JIM_I\rangle$ ground state to M_I substates of a $|JM_JIM_I\rangle$ excited state were not resolved.

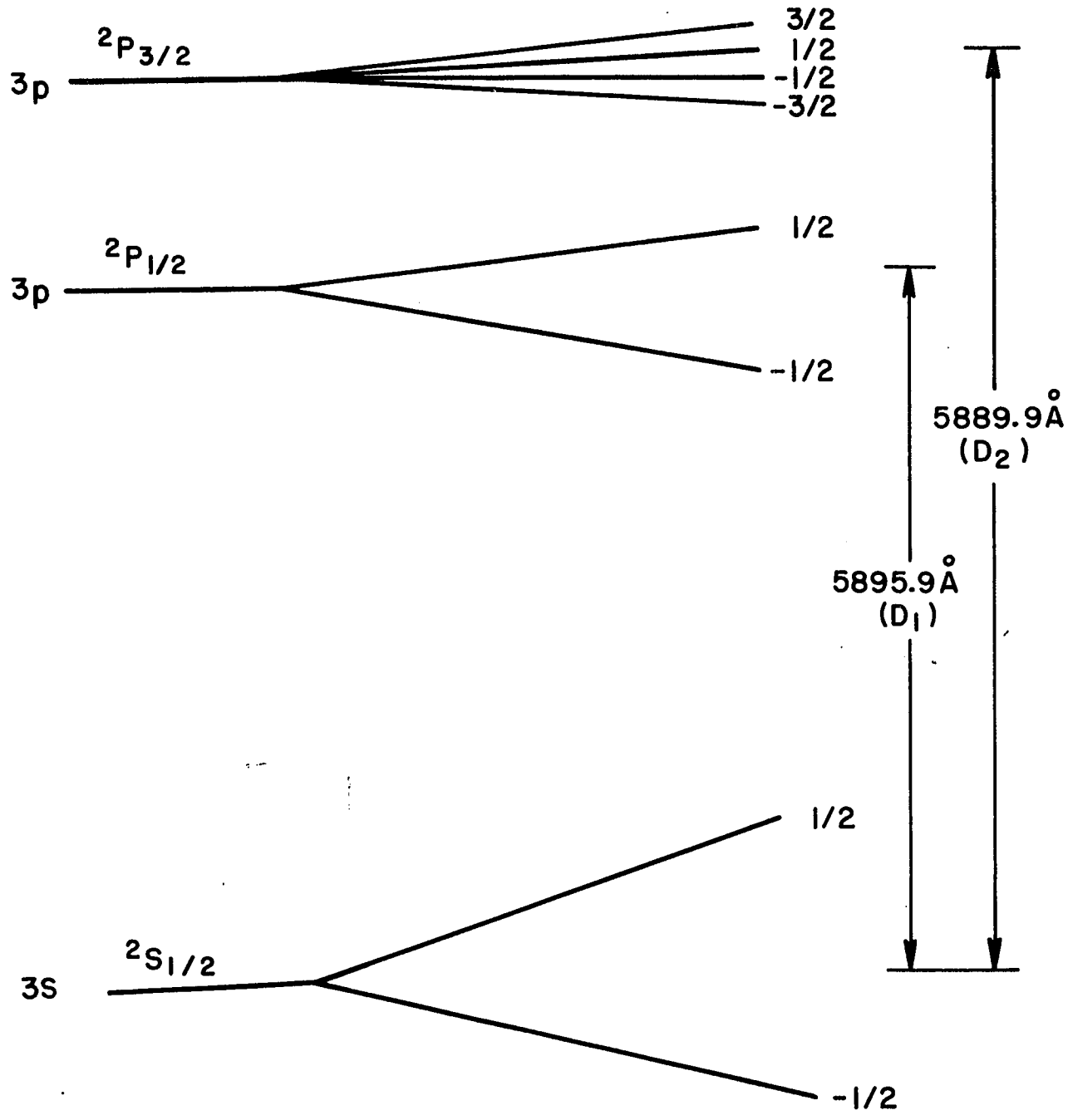
M_J (M_I = 3/2, 1/2, -1/2, -3/2)
$^2P_{3/2}$
3p
3/2
1/2
-1/2
-3/2
$^2P_{1/2}$
3p
1/2
-1/2
5889.9Å
(D_2)
5895.9Å
(D_1)
$^2S_{1/2}$
3S
1/2
-1/2

FIG. 8

Fig. 9. Hyperfine structure of Na

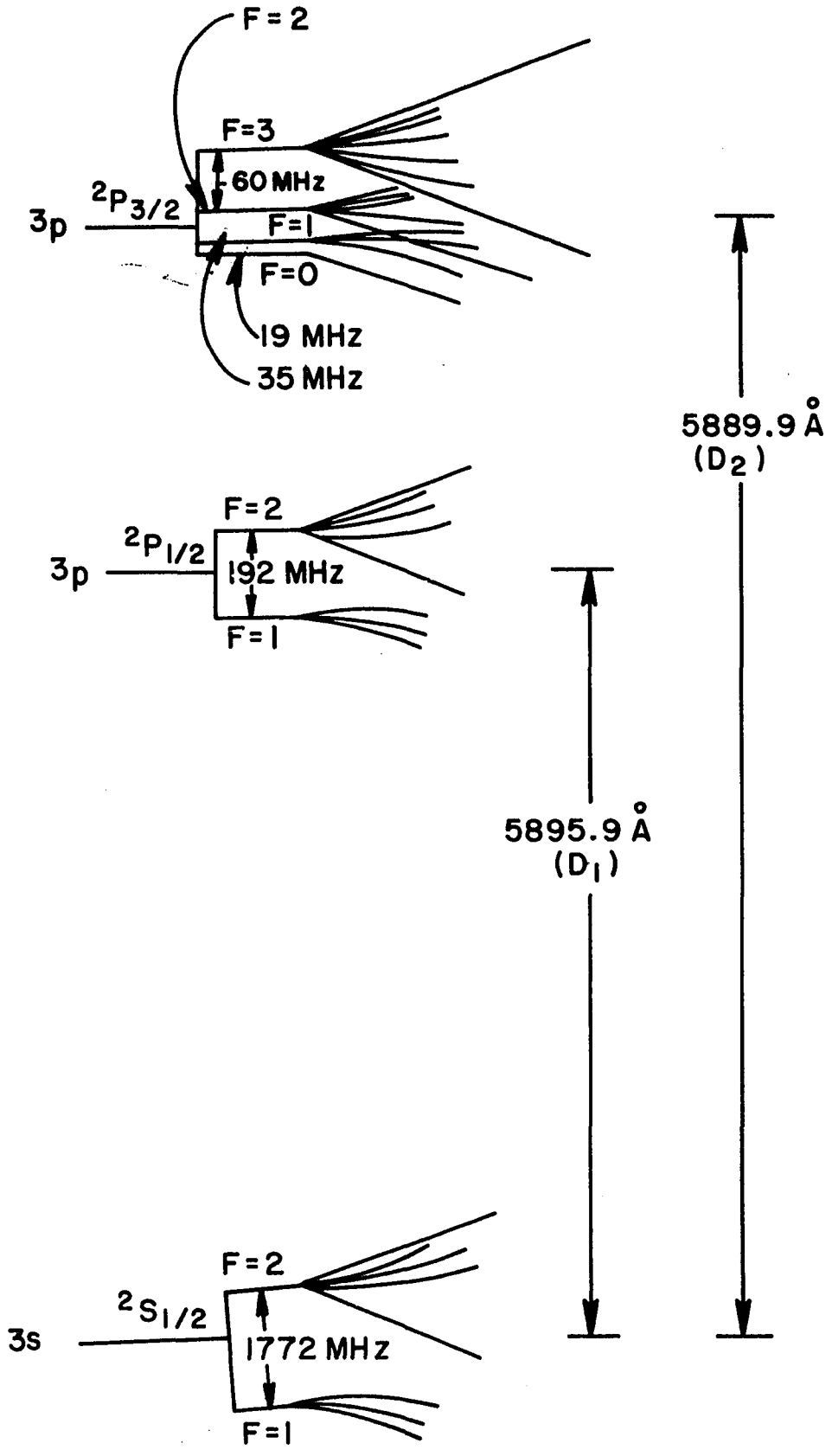
F = 2
F=3
60 MHz
$^2P_{3/2}$
3p
F=1
F=0
19 MHz
35 MHz
5889.9 Å
(D_2)
F=2
$^2P_{1/2}$
192 MHz
3p
F=1
5895.9 Å
(D_1)
F=2
$^2S_{1/2}$
1772 MHz
3s
F=1

FIG. 9

Fig. 10. Partial lifetimes of excited states in a large magnetic field for linearly (a and b) and circularly (c and d) polarized D_1 (b and c) and D_2 (a and b) transitions.

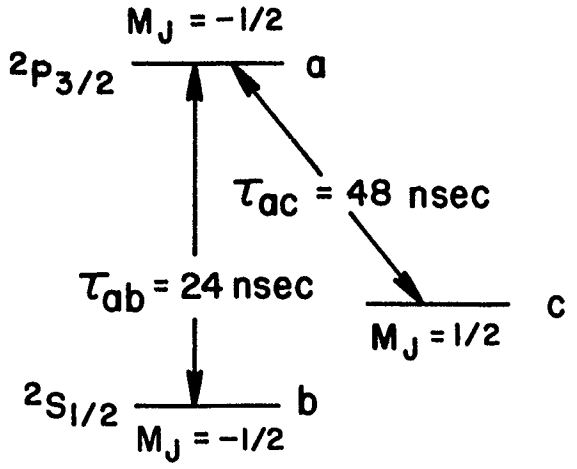
$M_J = -1/2$
$^2P_{3/2}$
a
τ_{ac} = 48 nsec
τ_{ab} = 24 nsec
c
$M_J = 1/2$
$^2S_{1/2}$
b
$M_J = -1/2$

(a)

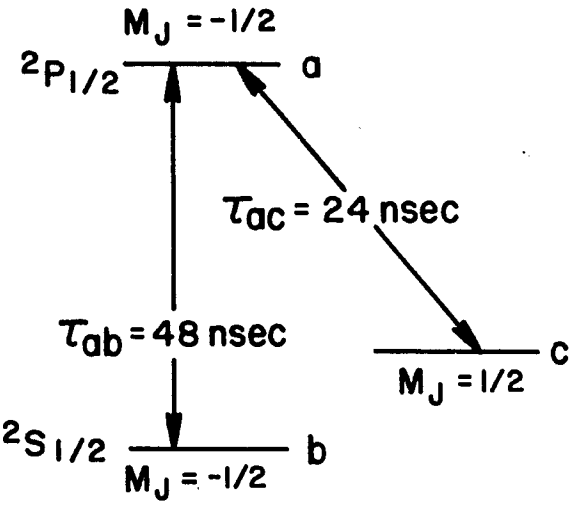
$M_J = -1/2$
$^2P_{1/2}$
a
τ_{ac} = 24 nsec
τ_{ab} = 48 nsec
c
$M_J = 1/2$
$^2S_{1/2}$
b
$M_J = -1/2$

(b)

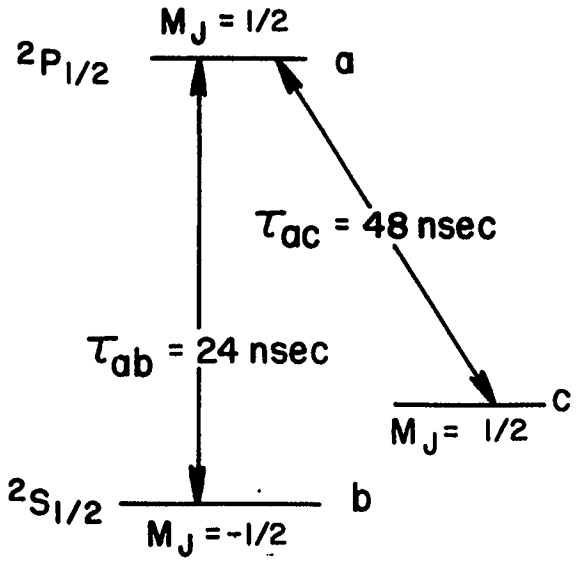
$M_J = 1/2$
$^2P_{1/2}$
a
τ_{ac} = 48 nsec
τ_{ab} = 24 nsec
c
$M_J = 1/2$
$^2S_{1/2}$
b
$M_J = -1/2$

(c)

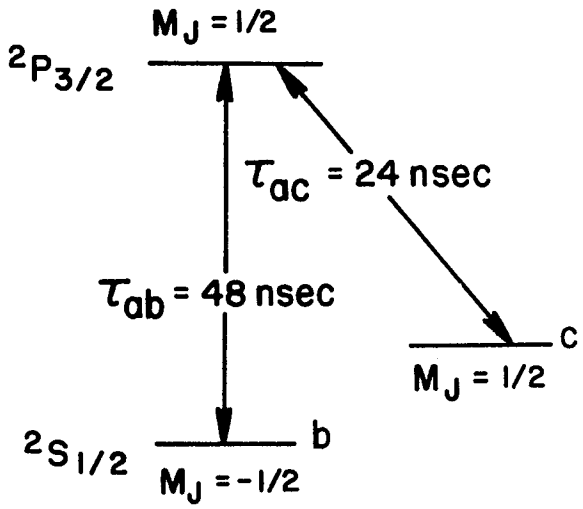
$M_J = 1/2$
$^2P_{3/2}$
τ_{ac} = 24 nsec
τ_{ab} = 48 nsec
c
$M_J = 1/2$
$^2S_{1/2}$
b
$M_J = -1/2$

(d)

FIG. 10

Fig. 11. Experimental output pulse shapes as seen for the D_1 transitions (a) and the D_2 transitions (b) for linearly polarized light in a large magnetic field.

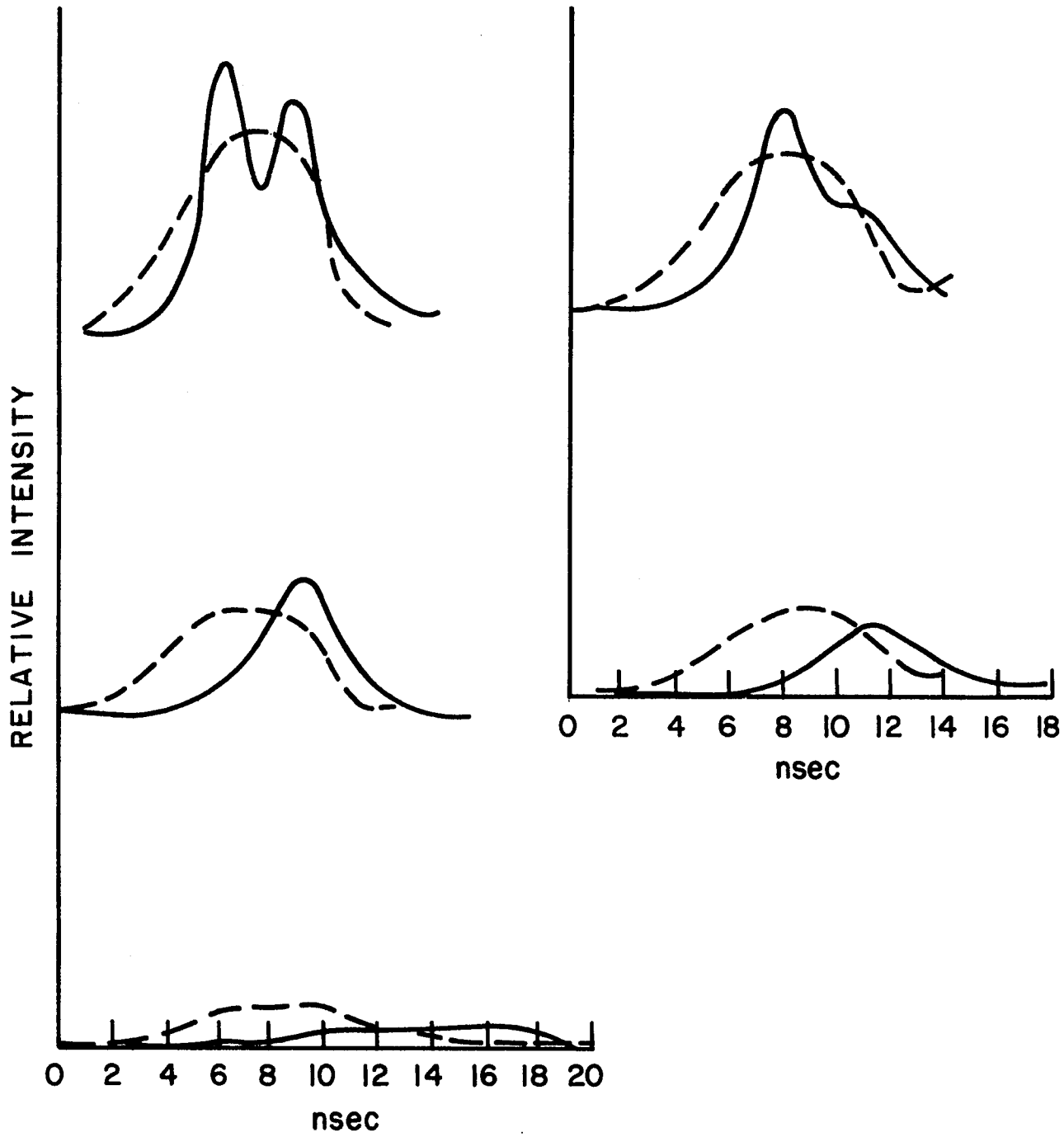
RELATIVE INTENSITY
0 2 4 6 8 10 12 14 16 18 20
nsec
0 2 4 6 8 10 12 14 16 18
nsec

FIG. 11 (a)

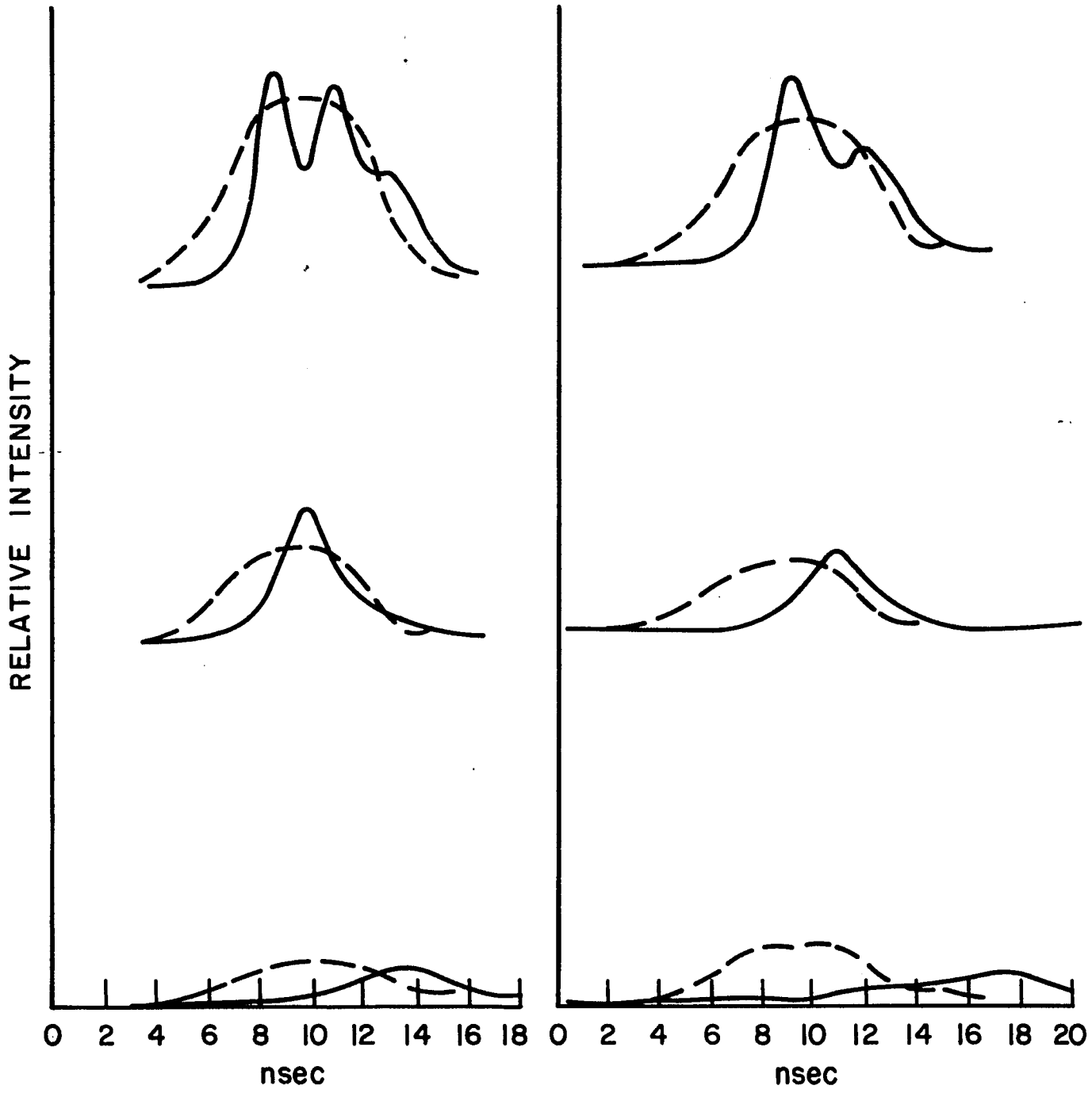
RELATIVE INTENSITY
0 2 4 6 8 10 12 14 16 18
nsec
0 2 4 6 8 10 12 14 16 18 20
nsec

FIG. 11 (b)

Fig. 12. Data for circularly polarized transitions for

(a) $^2S_{1/2}(M_J=-1/2)$ to $^2P_{1/2}(M_J=1/2)$;

(b) $^2S_{1/2}(M_J=-1/2)$ to $^2P_{3/2}(M_J=1/2)$; and

(c) $^2S_{1/2}(M_J=1/2)$ to $^2P_{3/2}(M_J=3/2)$.

Experimentally, the predicted differences in the transition dipole moments for these three transitions were observed. For the same input pulse, the output pulse on the D_1 transition exhibited characteristic 4π breakup while the $^2S_{1/2}(M_J=-1/2)$ to $^2P_{3/2}(M_J=1/2)$ D_2 transition exhibited 3π characteristic breakup and the $^2S_{1/2}(M_J=1/2)$ to $^2P_{3/2}(M_J=3/2)$ D_2 transition exhibited characteristic 6π breakup.

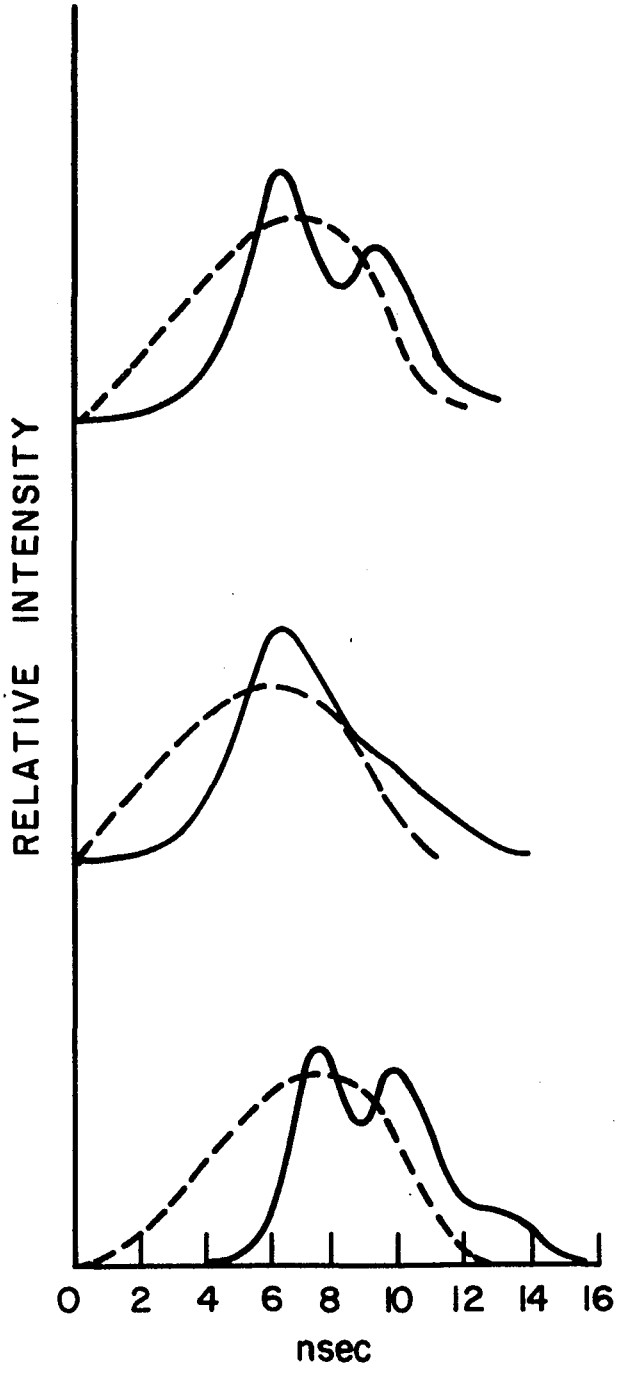

FIG. 12

Fig. 13. Allowed D_1 transitions in a weak magnetic field for light linearly polarized parallel to the magnetic field and wave vector perpendicular to the magnetic field.

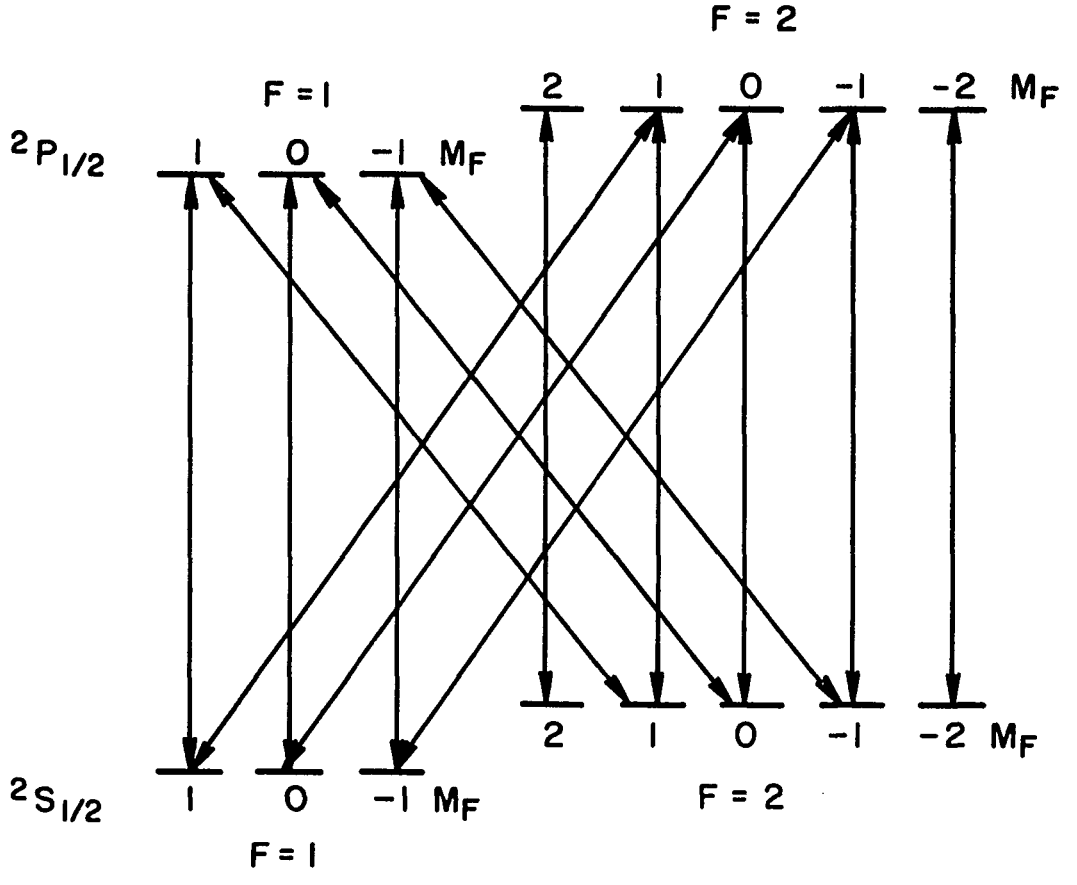

FIG. 13

Fig. 14. Output pulse shapes (a), allowed transitions (b), S(A) curve (c), W(A) curve (d), and F(A) curve (e) with the laser tuned (900 MHz off center) to the low frequency side (F=2) of the D_1 transition in a weak magnetic field. Pulse breakup is nearly as sharp as in the nondegenerate case (Fig. 11). Likewise the curves S(A), W(A), and F(A) do not deviate much from similar nondegenerate curves (Fig. 22).

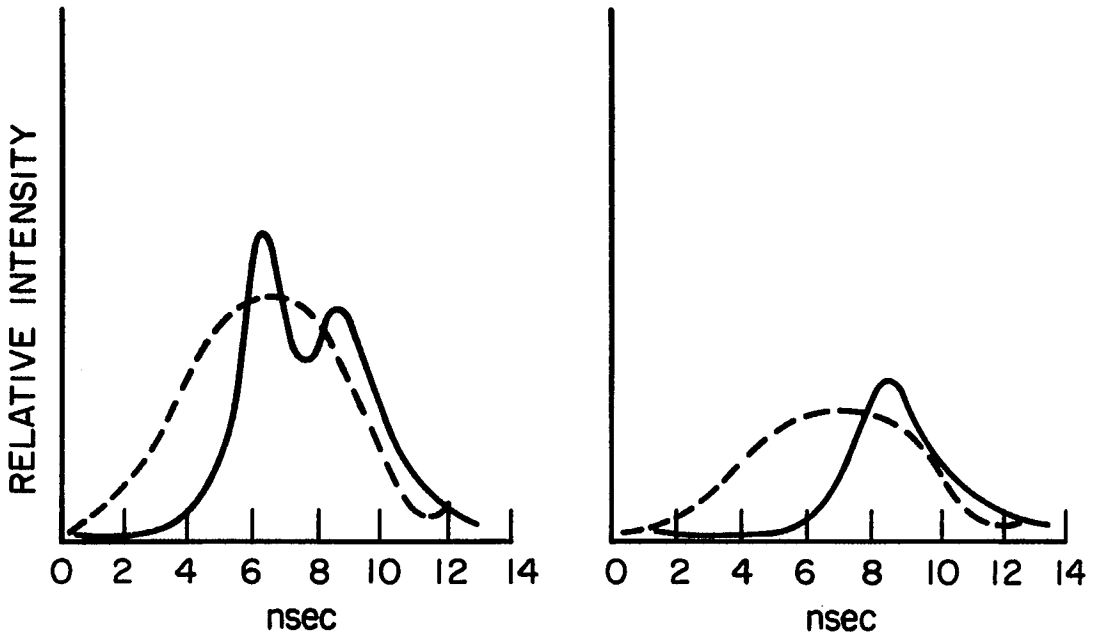

(a)

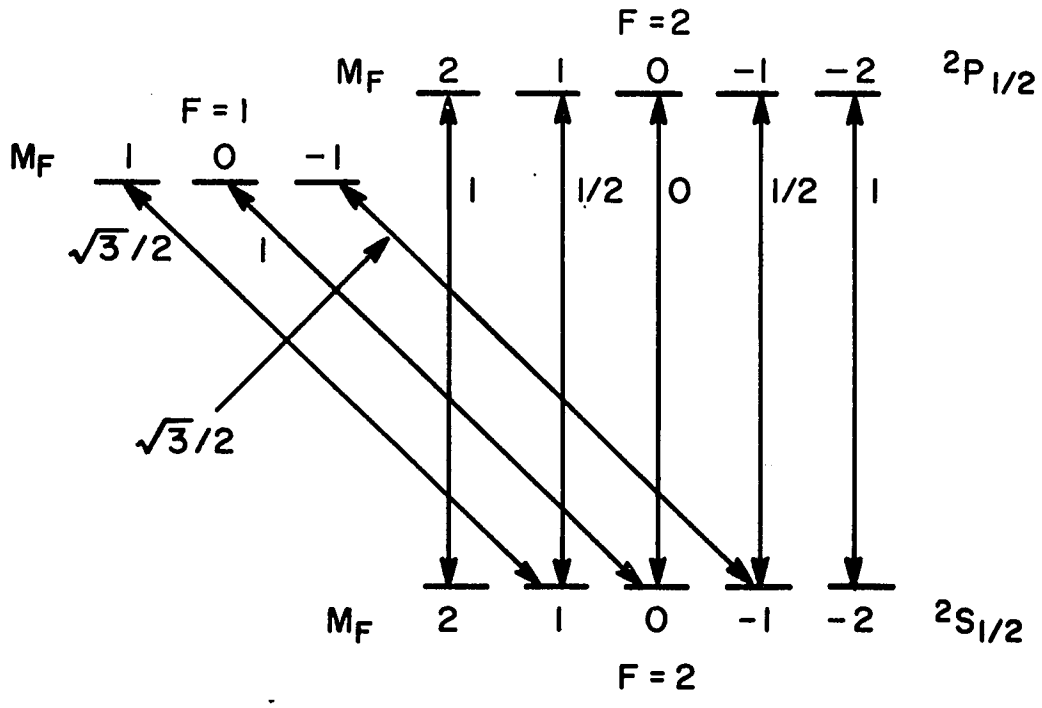

(b)

FIG. 14 (a AND b)

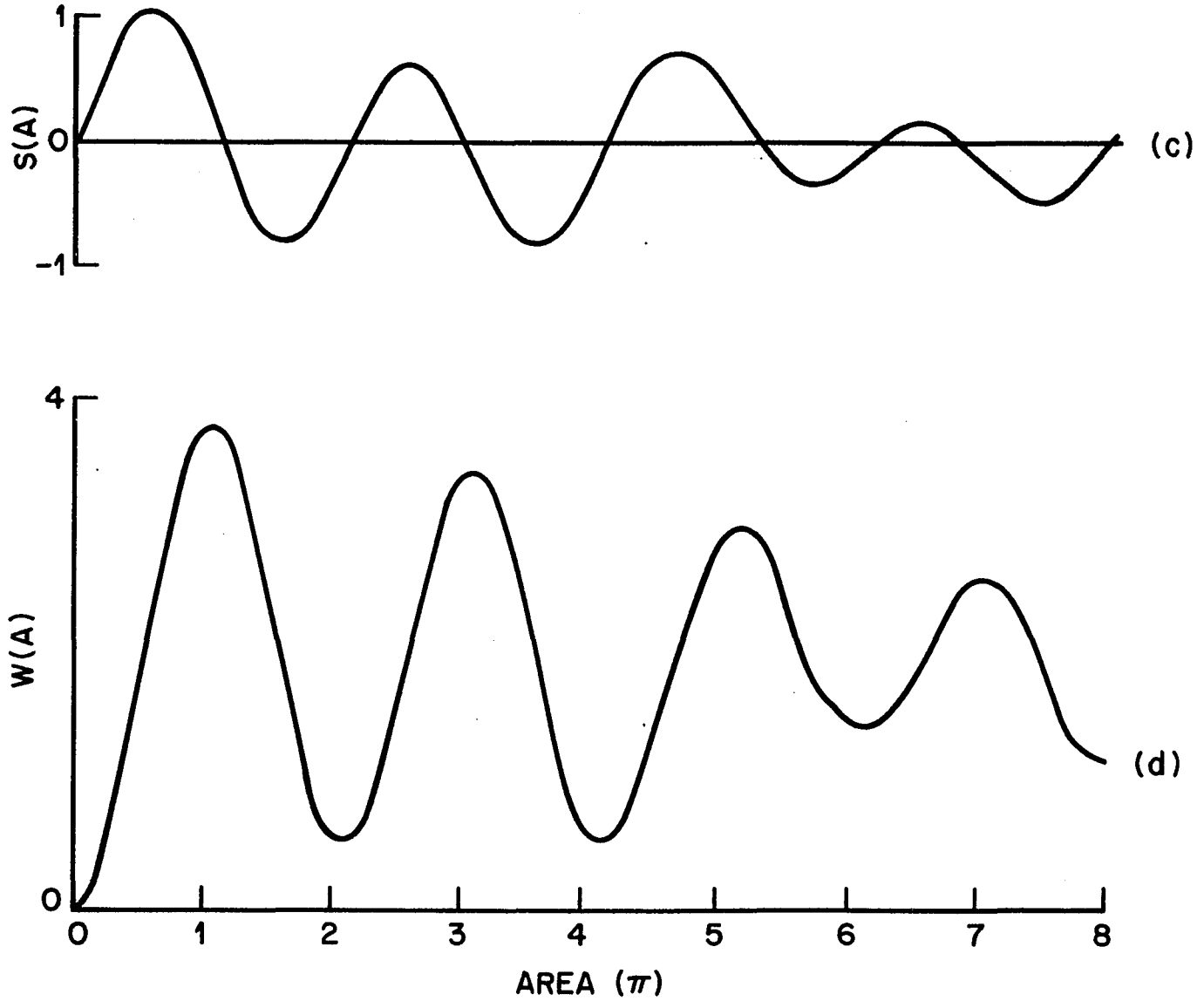

FIG. 14 (c AND d)

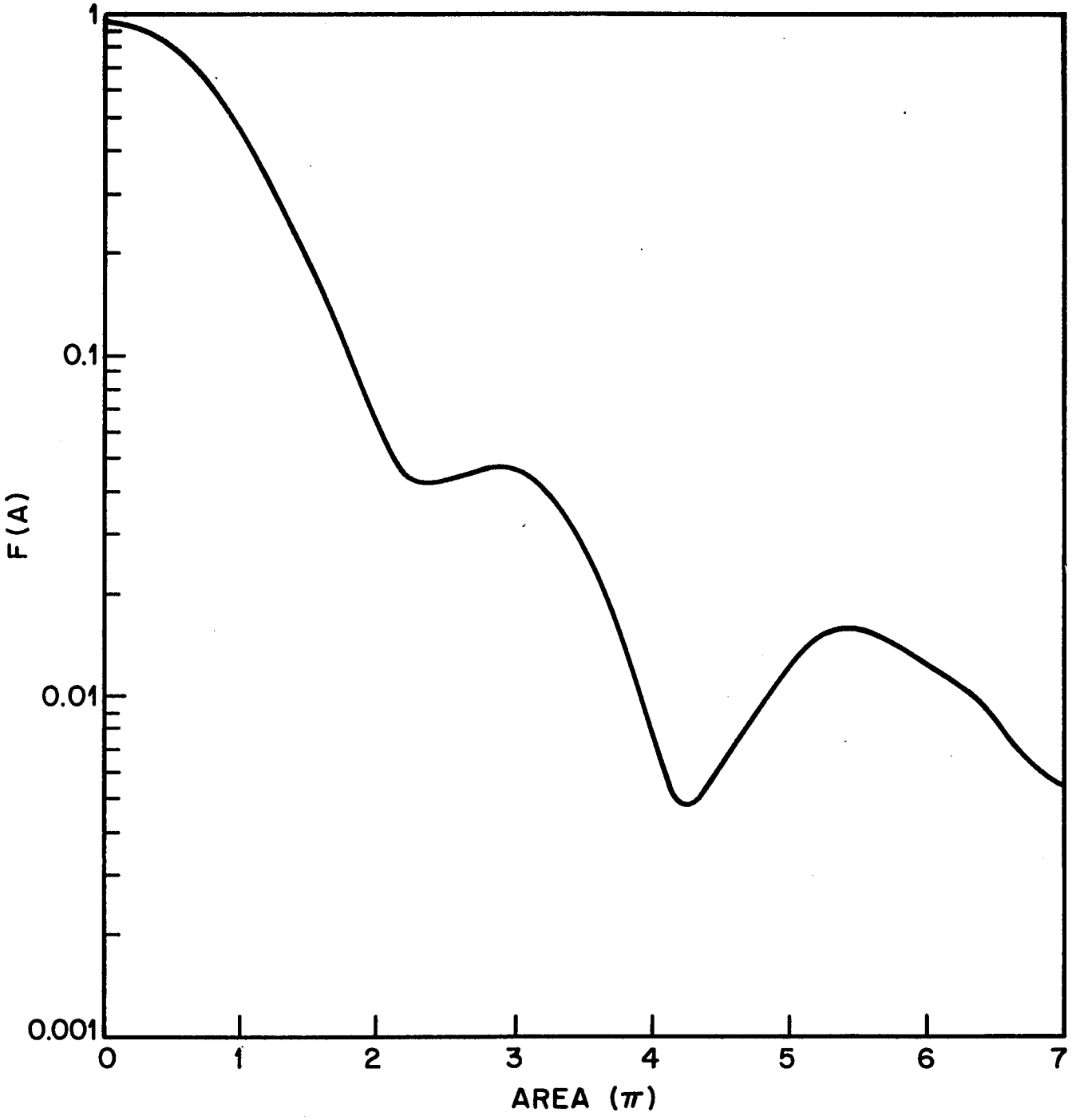

FIG. 14 (e)

Fig. 15. Output pulse shapes (a), allowed transitions (b), S(A) curve (c), W(A) curve (d), and F(A) curve (e) with the laser tuned to the center of the D_1 transition in a weak magnetic field (F=1 and F=2). Pulse breakup looks slightly diminished relative to the low frequency side (Fig. 14) but still sharp. Nor do the theoretical curves S(A), W(A), or F(A) differ much either.

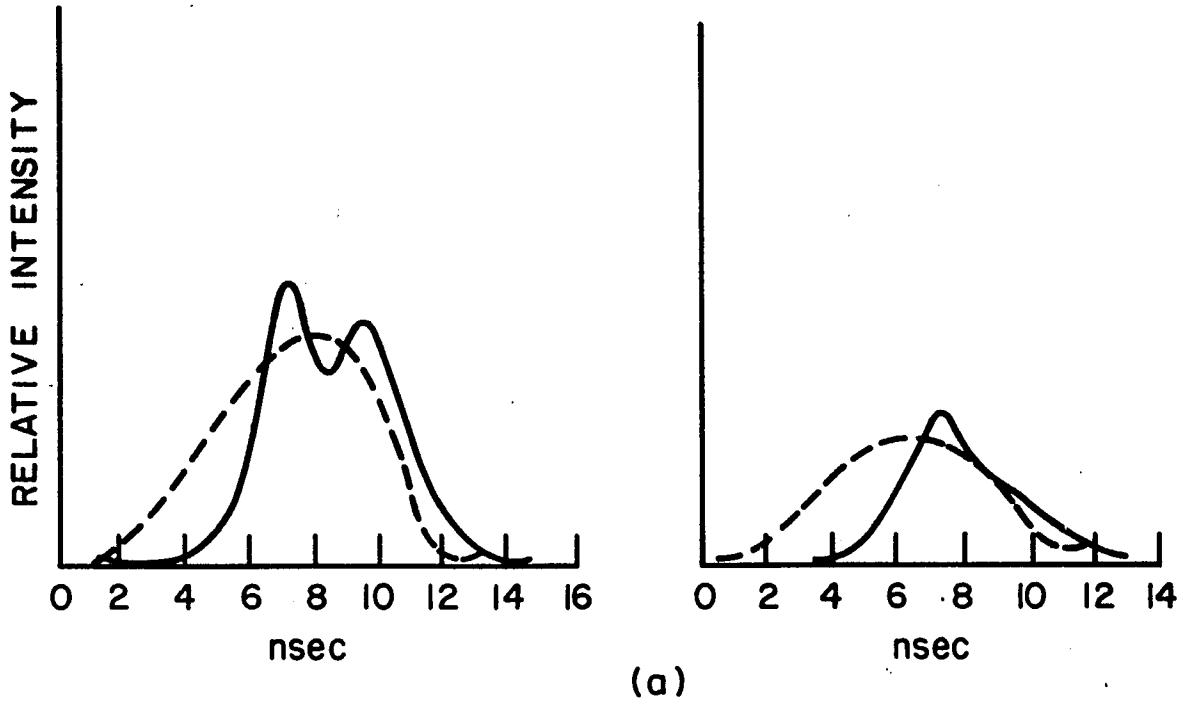

(a)

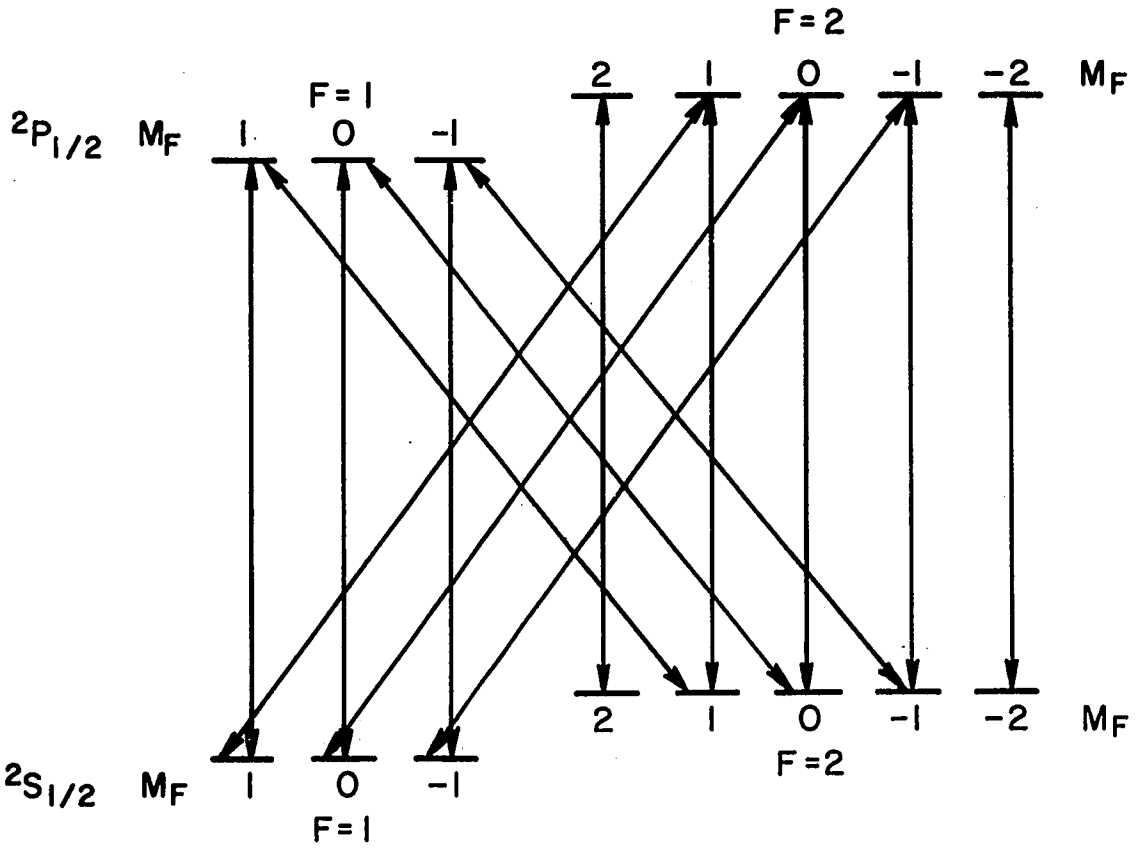

(b)

FIG. 15 (a AND b)

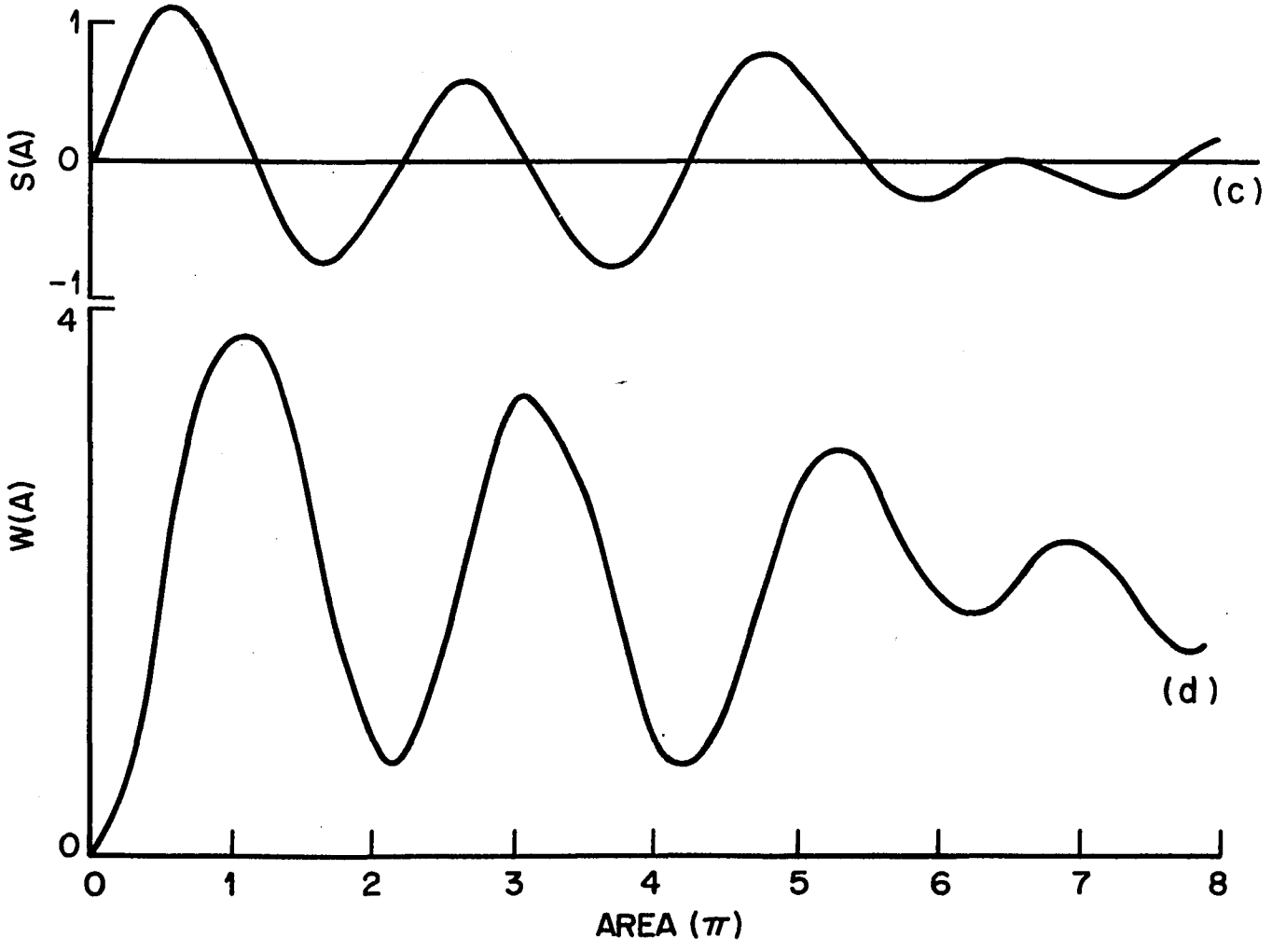

FIG. 15 (C AND d)

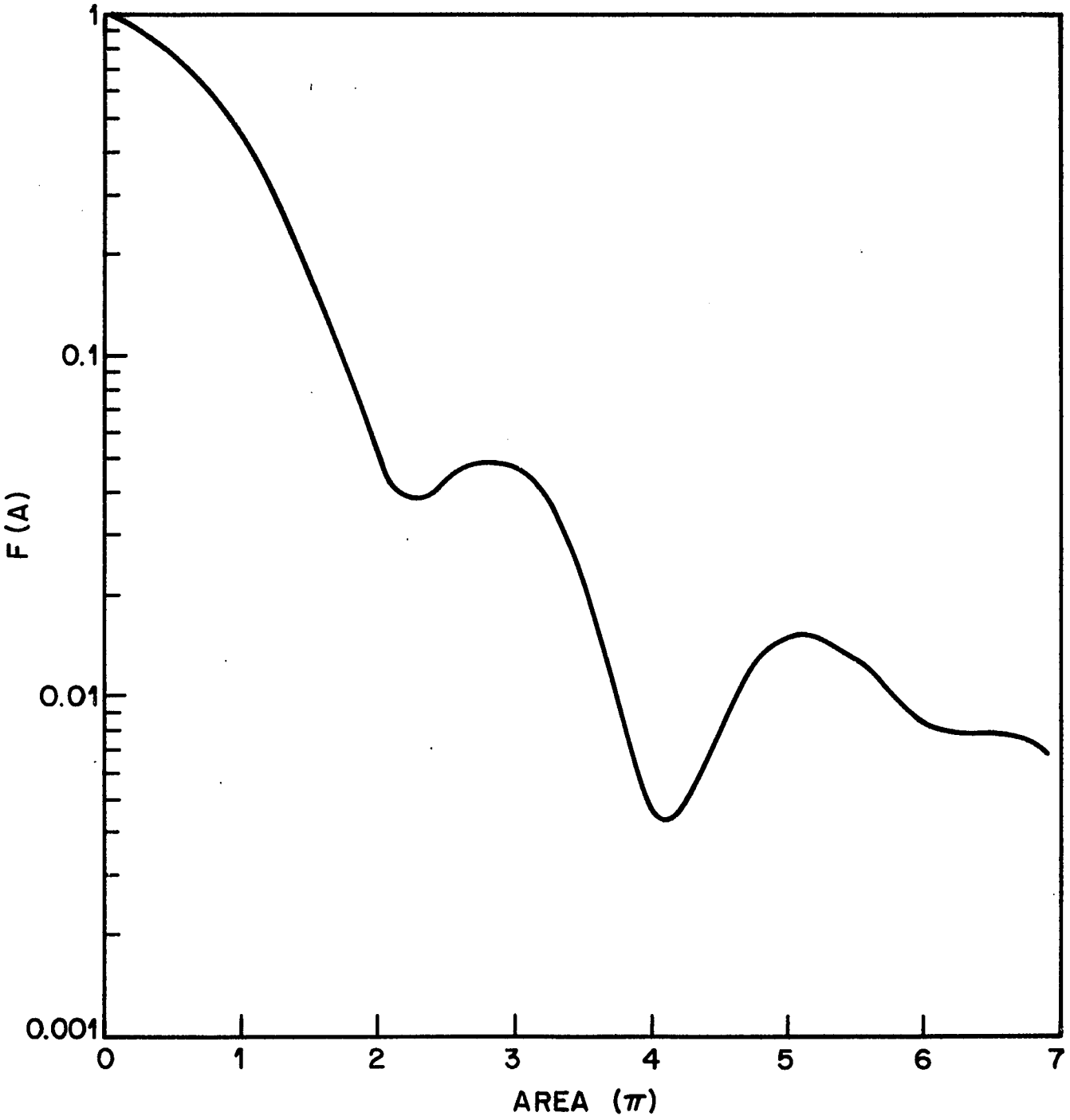

FIG. 15 (e)

Fig. 16. Output pulse shapes (a), allowed transitions (b), S(A) curve (c), W(A) curve (d), and F(A) curve (e) with the laser tuned (900 MHz off center) to the high frequency side (F=1) of the D_1 transition. Pulse breakup is further diminished, but is clearly present. The curves S(A), W(A), and F(A) do not deviate much from those for the low frequency side of the D_1 transition (Fig. 14). But for the same temperature one would expect less reshaping, i.e. less pronounced breakup, for the high frequency side which has an αL only 3/5 that of the low frequency side.

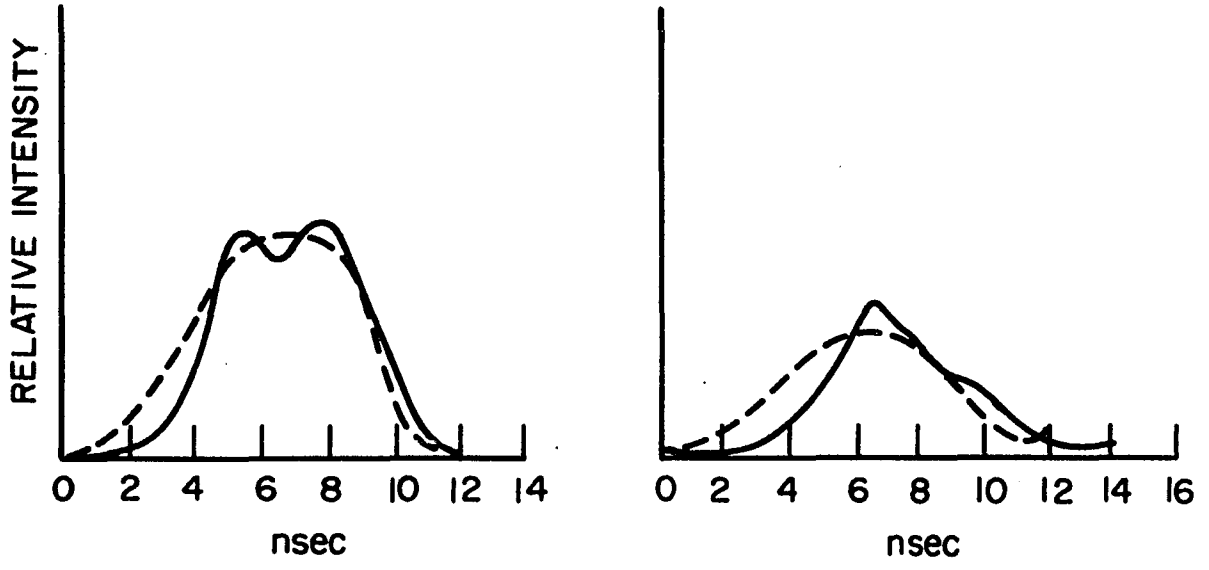

(a)

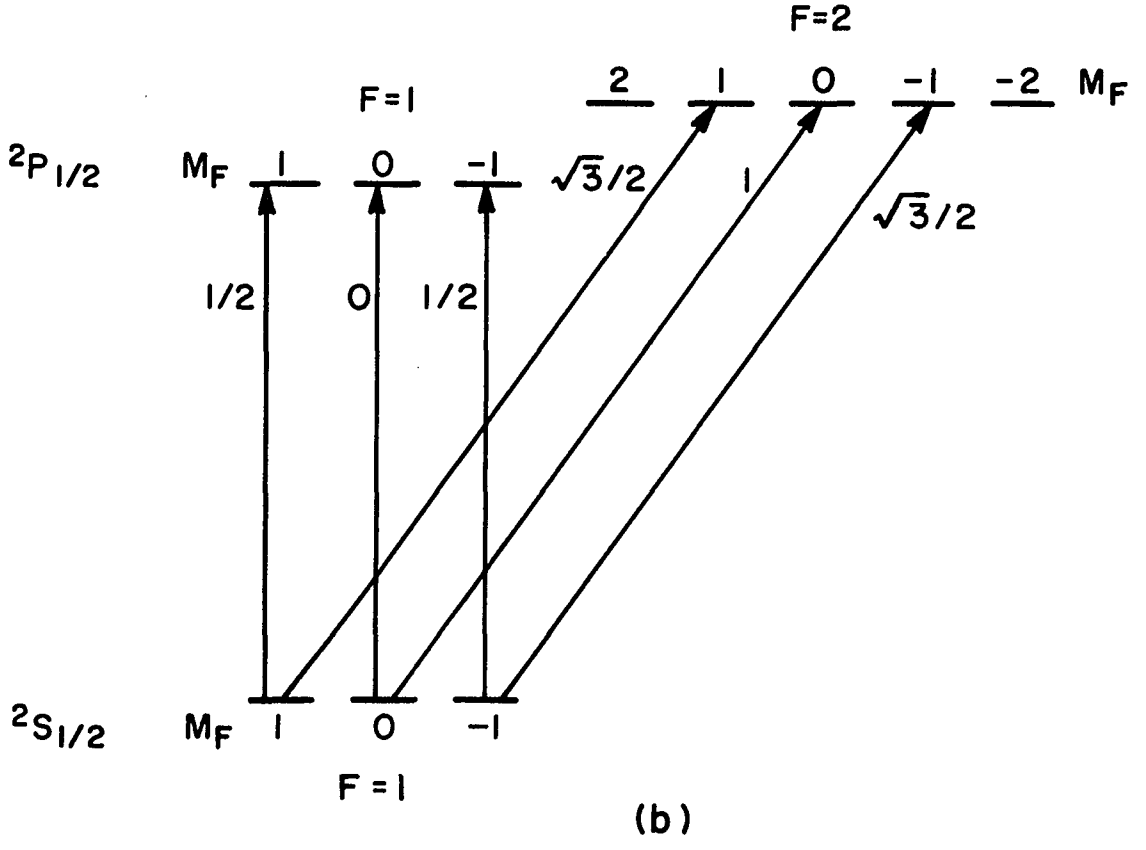

(b)

FIG. 16 (a AND b)

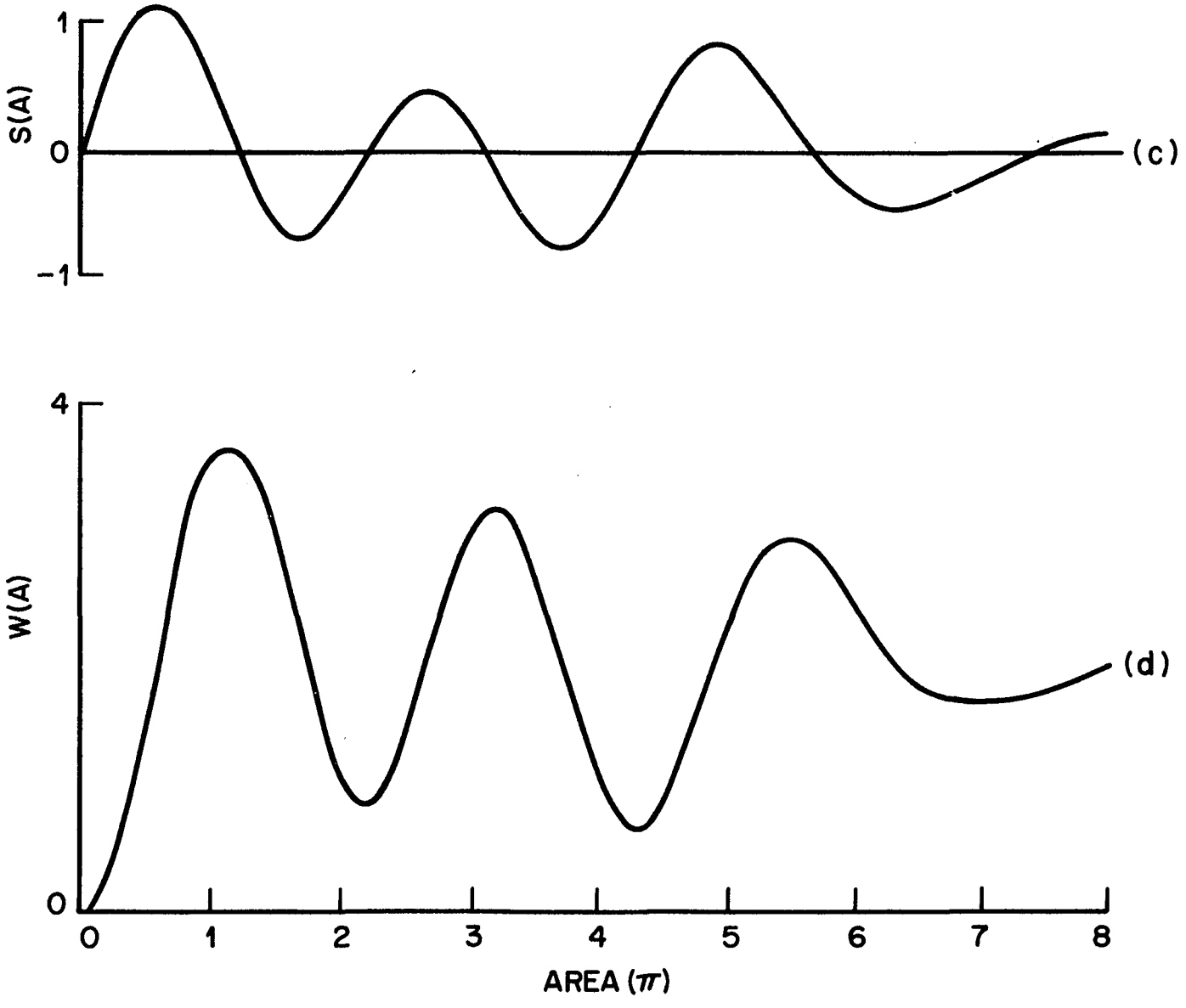

FIG. 16 (c AND d)

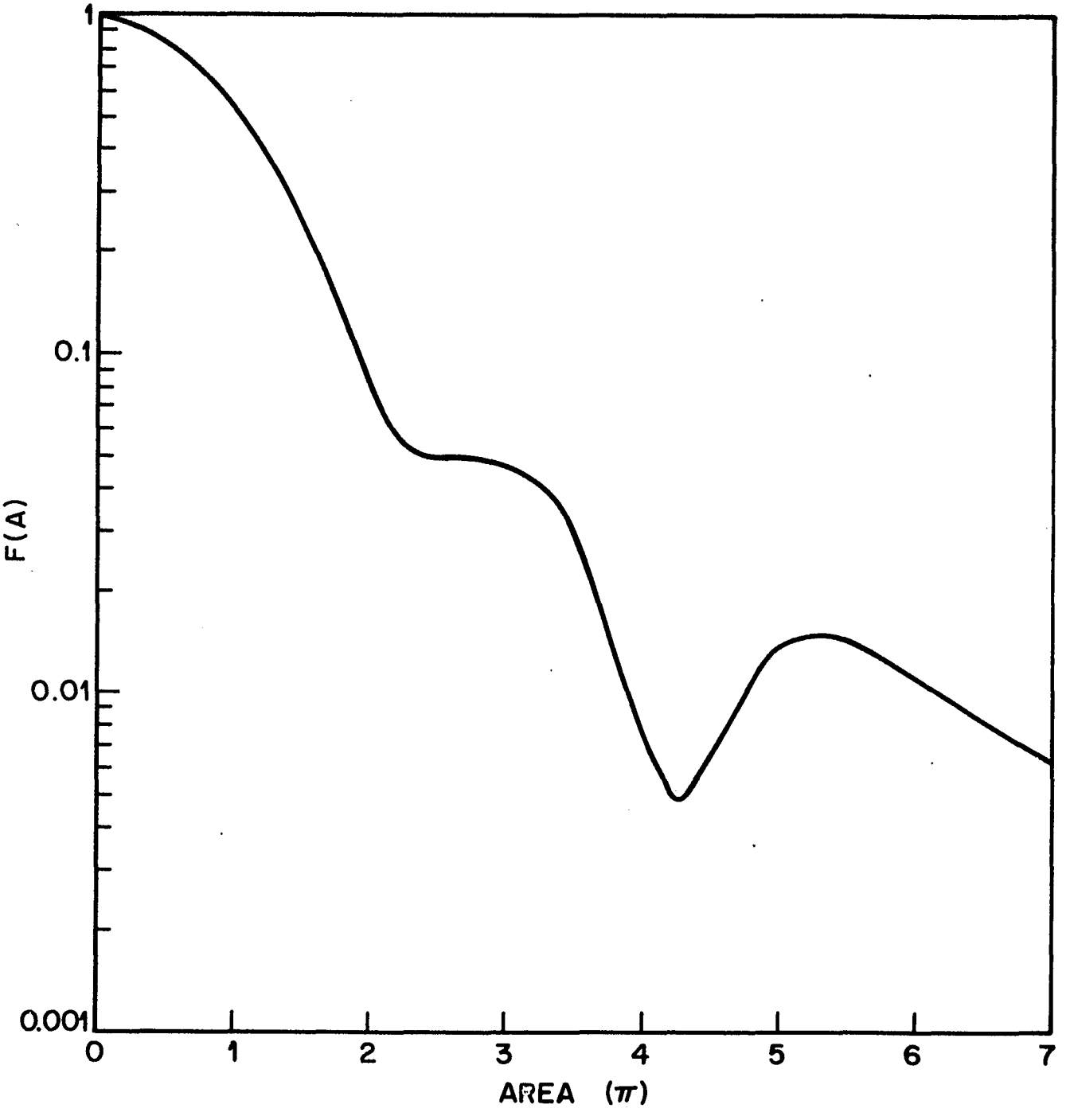

FIG. 16 (e)

Fig. 17. Output pulse shapes with the laser tuned to the high-frequency side of the D_1 transition with αL increased. Pulse breakup is shown to have improved.

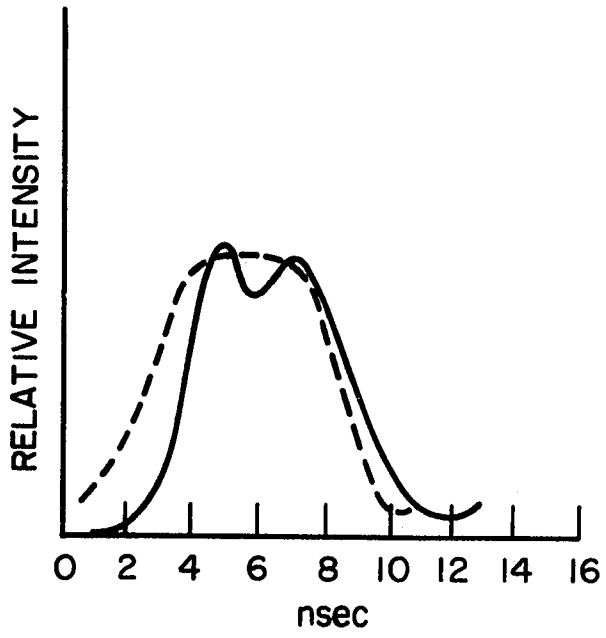

FIG. 17

Fig. 18. Allowed D_2 transitions in a weak magnetic field for light linearly polarized parallel to the magnetic field and wave vector perpendicular to the magnetic field.

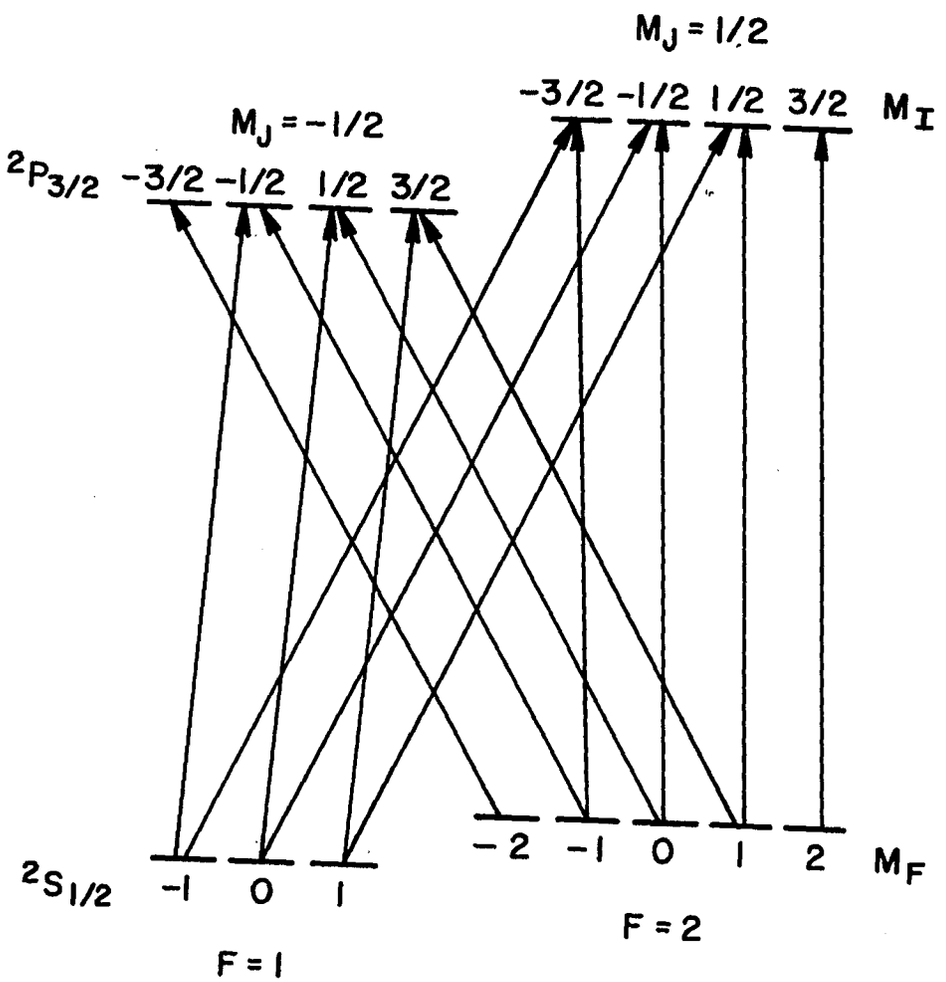

FIG. 18

Fig. 19. Output pulse shapes (a), allowed transitions (b), S(A) curve (c), W(A) curve (d), and F(A) curve (e) with the laser tuned (900 MHz off center) to the high-frequency side (F=1) of the D_2 transition in a magnetic field of 60 to 150 Gauss. Pulse breakup, although diminished relative to the D_1 transition in a weak magnetic field, is somewhat present. The curves S(A) and F(A) do not deviate much from those of the D_1 transition in a weak magnetic field. However, the W(A) curve does indicate smaller oscillations in the energy stored in the atoms. Pulse breakup therefore, is expected to be diminished.

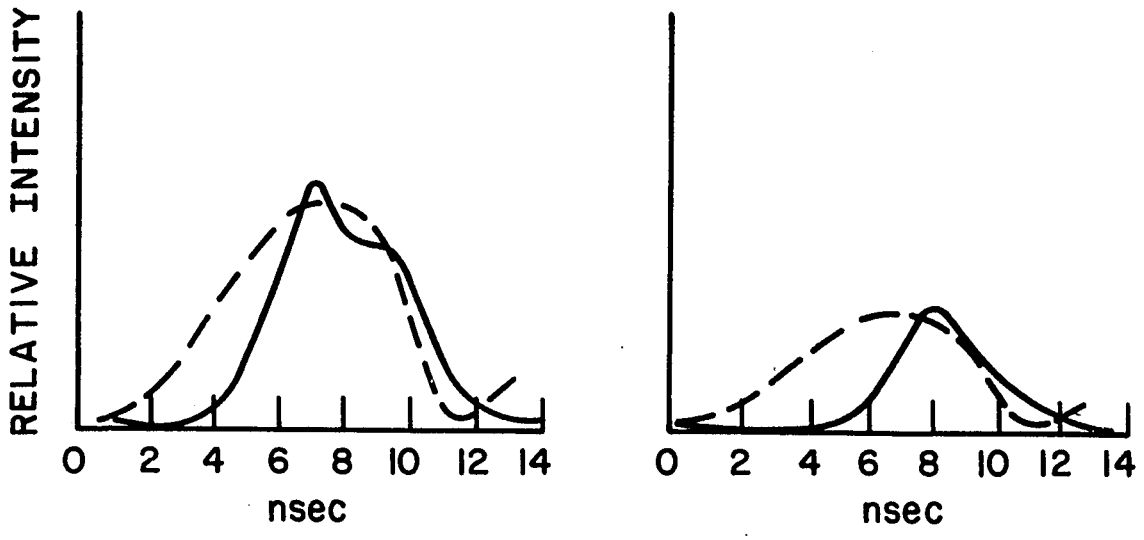

(a)

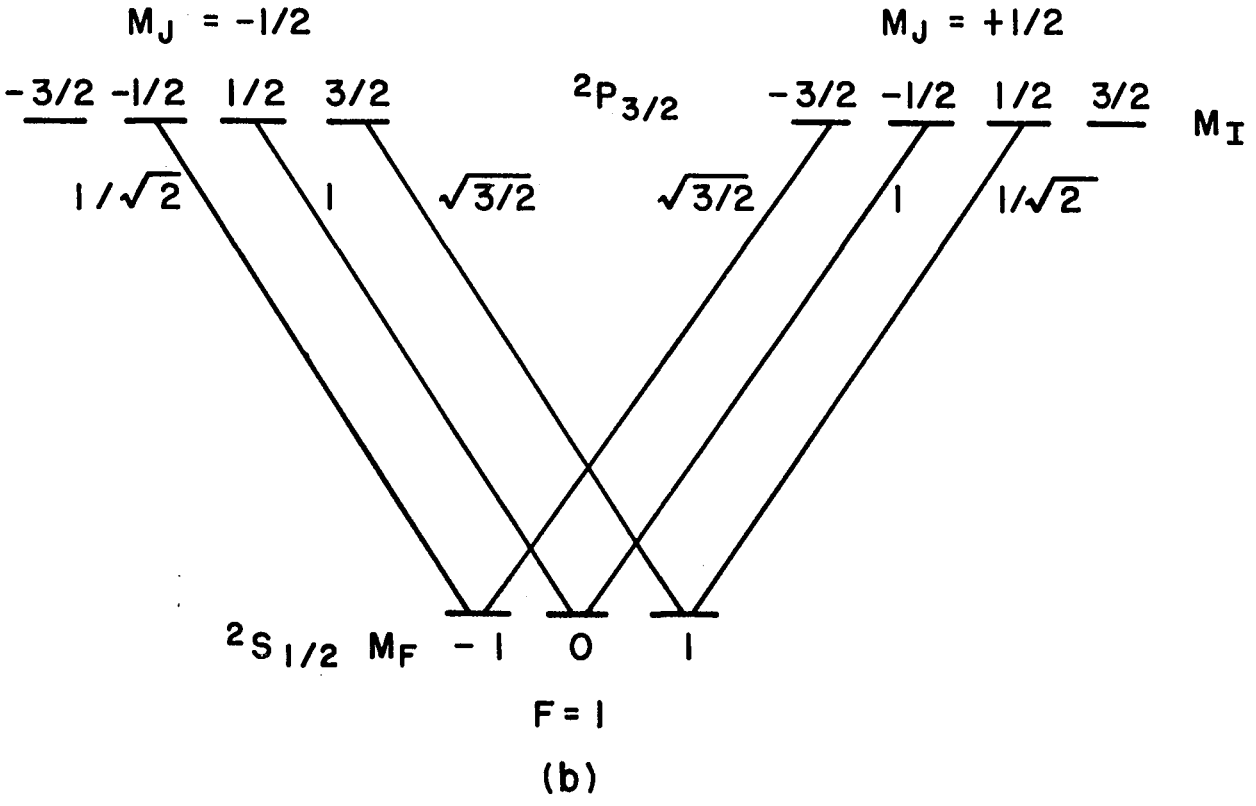

(b)

FIG. 19 (a AND b)

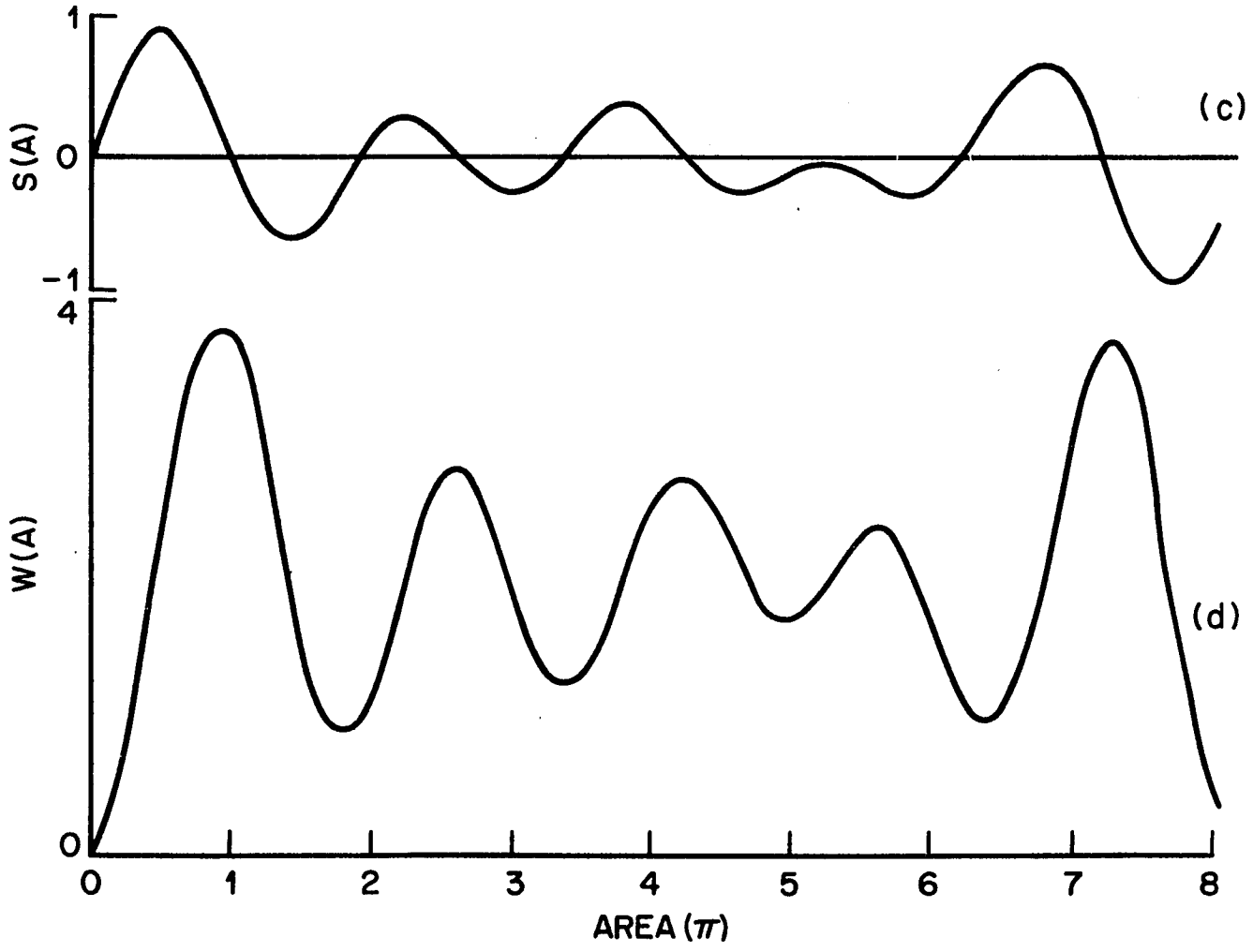

FIG. 19 (c AND d)

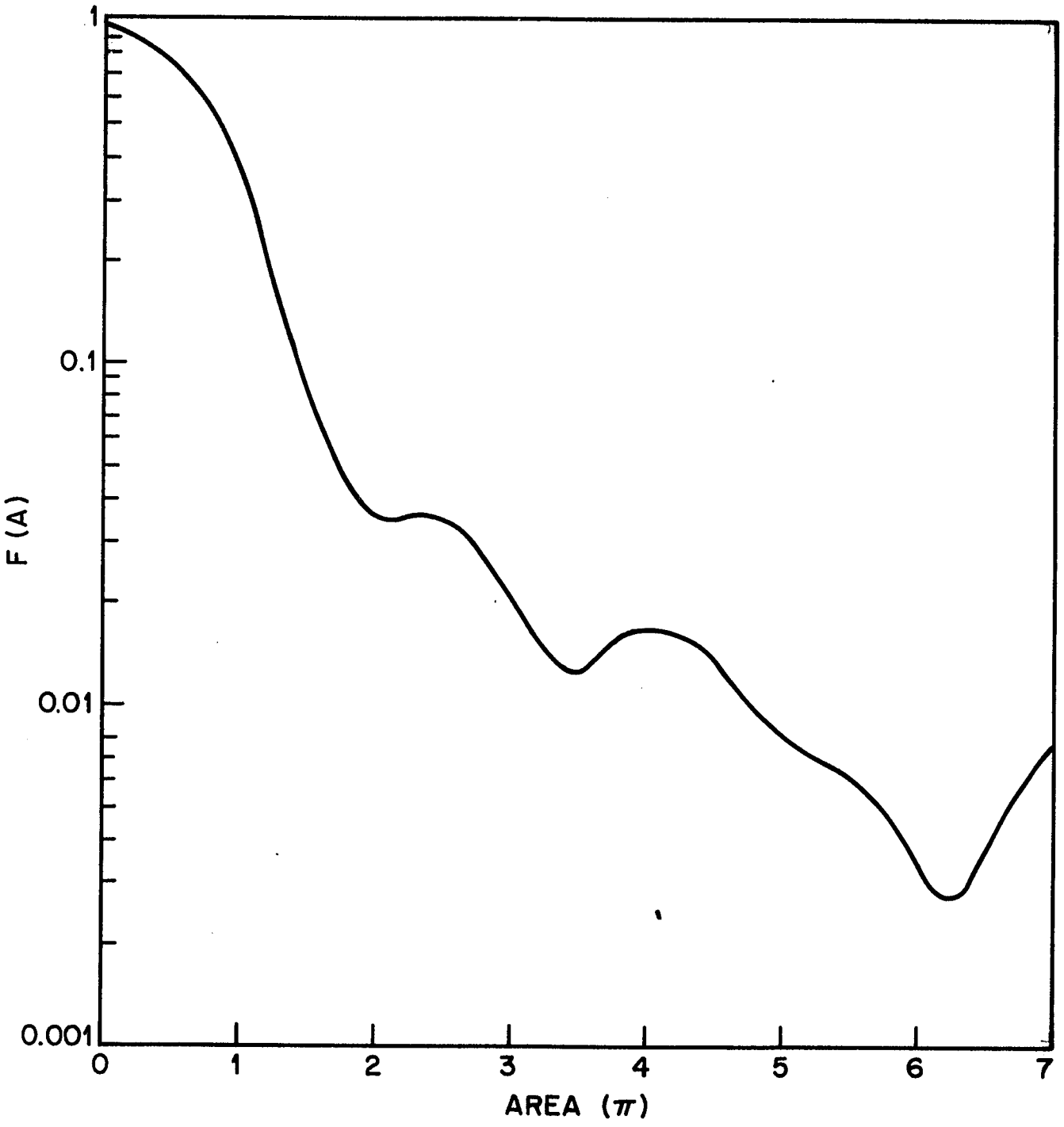

FIG. 19 (e)

Fig. 20. Output pulse shapes (a), allowed transitions (b), S(A) curve (c), W(A) curve (d), and F(A) curve (e) with the laser tuned (1800 MHz off center) to the low frequency side of the D_2 transition in a magnetic field between 60 and 150 Gauss. Pulse breakup is less pronounced than on the high-frequency side (Fig. 19) but the difference is small. Likewise, the curves S(A), F(A), and W(A) do not deviate much either.

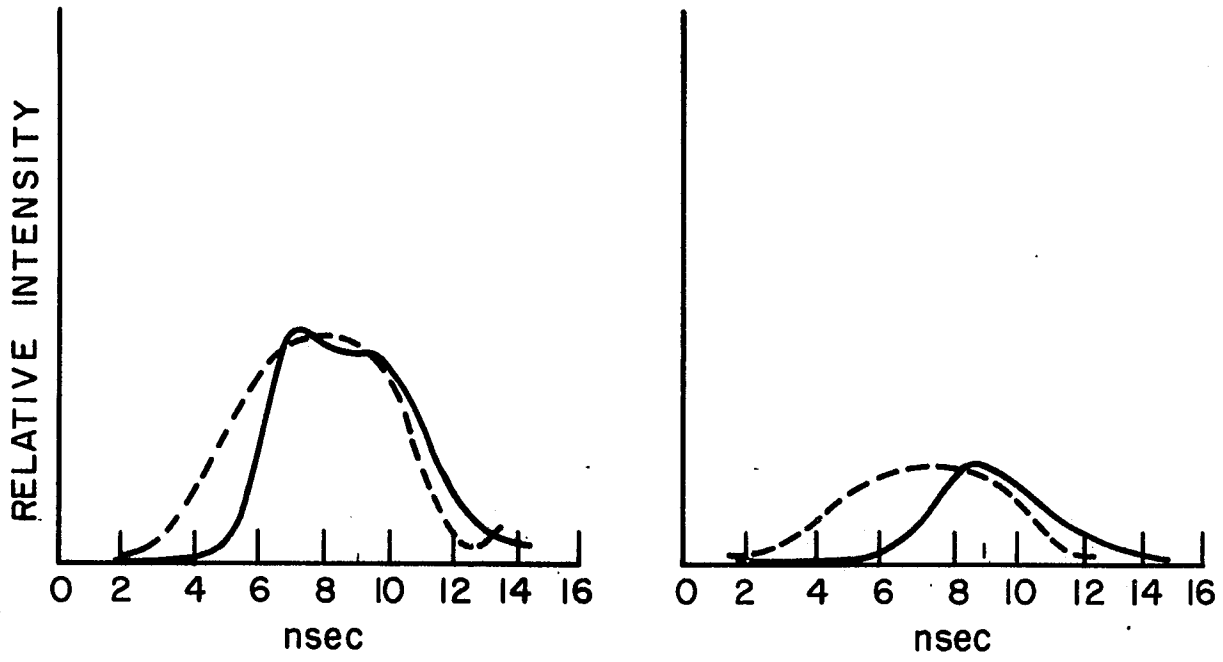

(a)

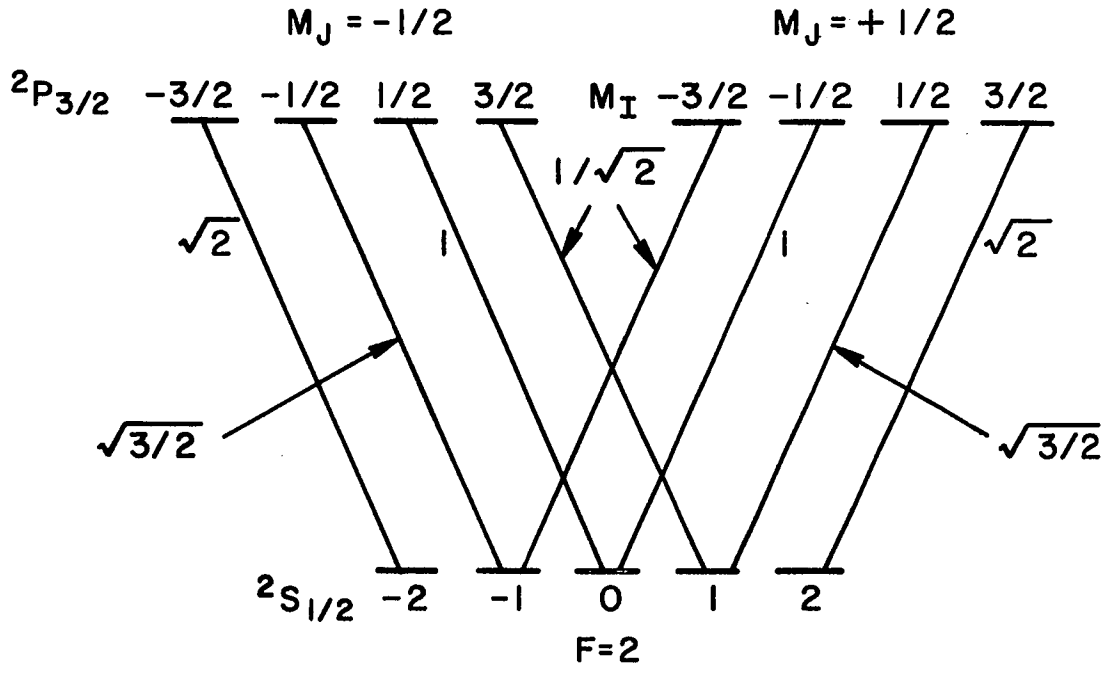

(b)

FIG. 20 (a AND b)

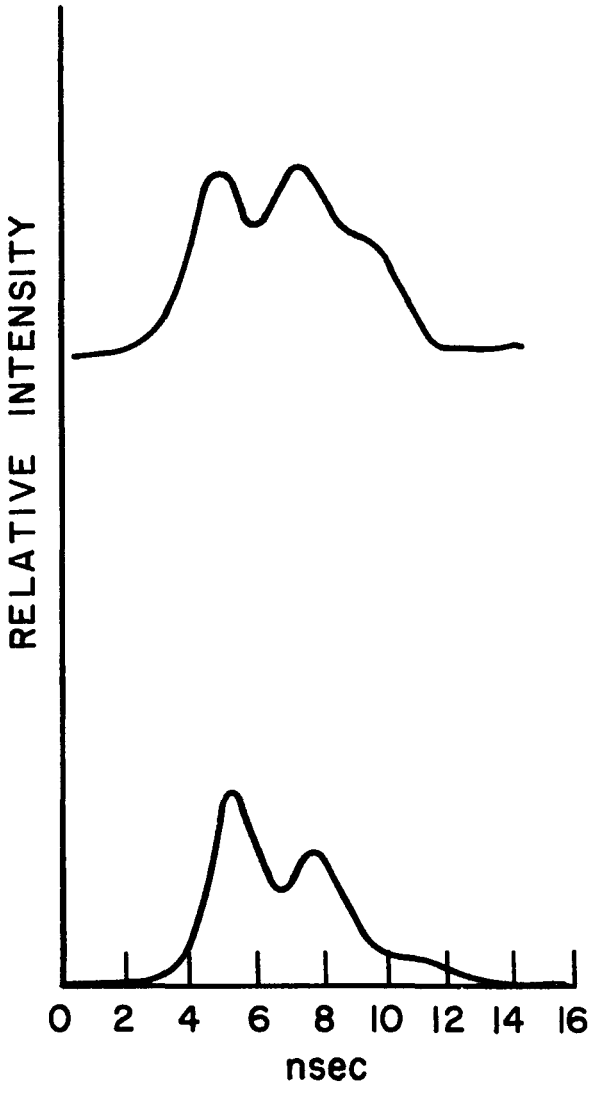

FIG. 21 (a)

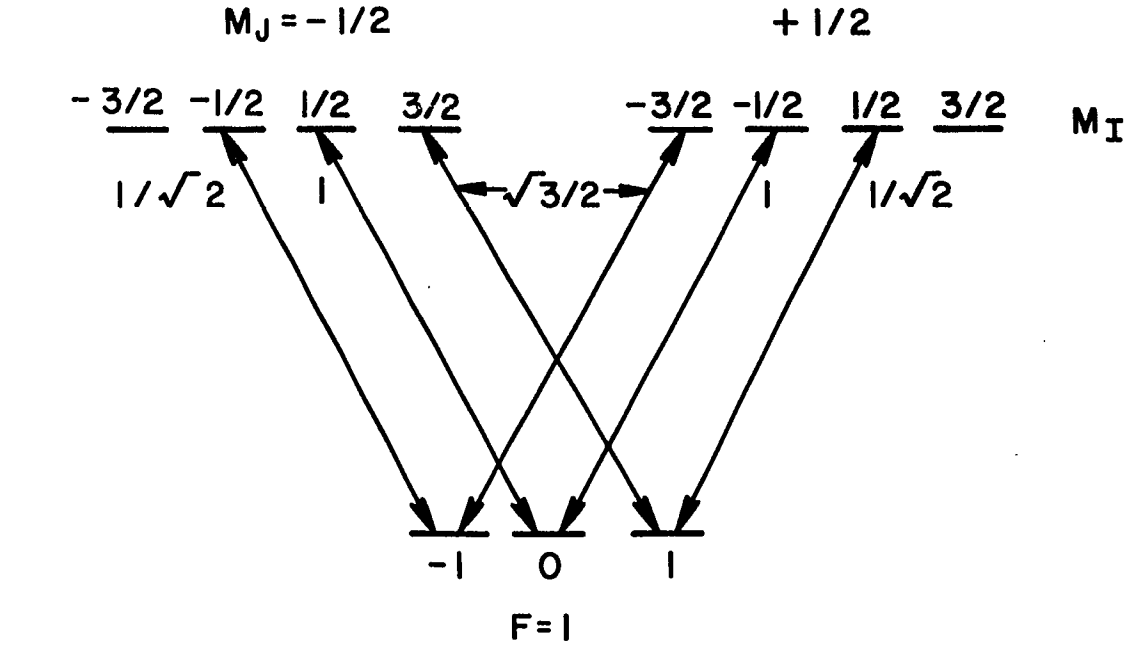
$M_J = -1/2$
$+1/2$
$-3/2$ $-1/2$ $1/2$ $3/2$
$-3/2$ $-1/2$ $1/2$ $3/2$
M_I
$1/\sqrt{2}$
1
$\sqrt{3/2}$
1
$1/\sqrt{2}$
-1 0 1
F=1

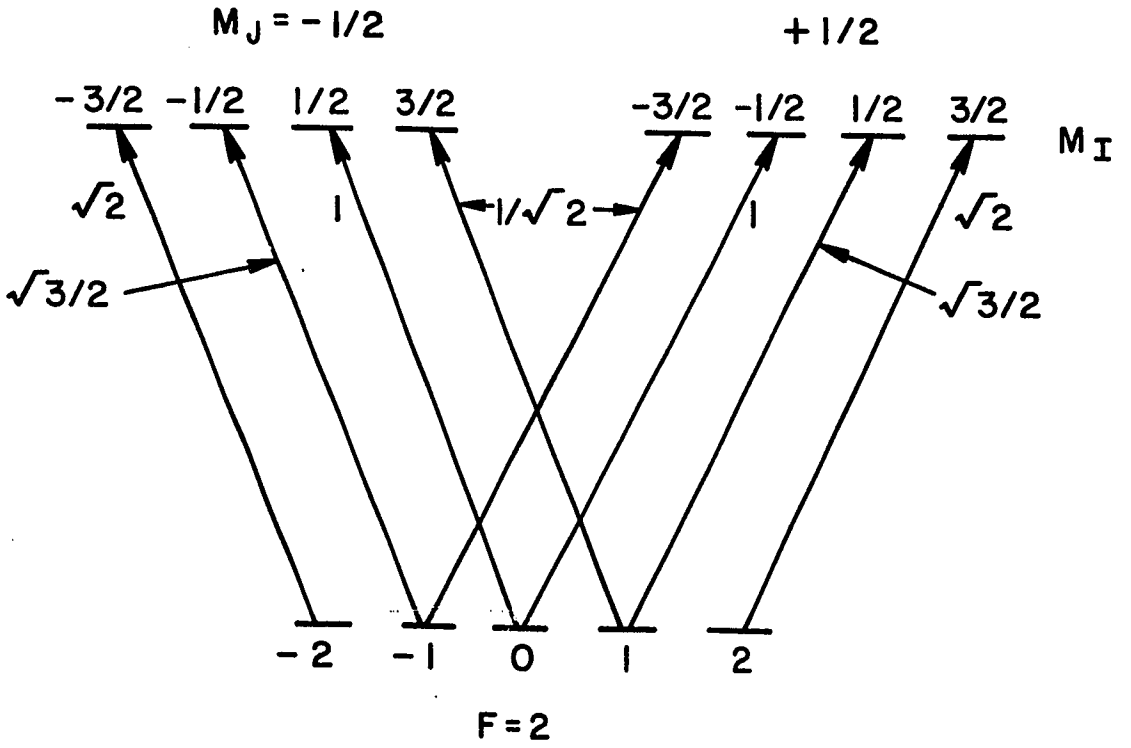
$M_J = -1/2$
$+1/2$
$-3/2$ $-1/2$ $1/2$ $3/2$
$-3/2$ $-1/2$ $1/2$ $3/2$
M_I
$\sqrt{2}$
$\sqrt{3/2}$
1
$1/\sqrt{2}$
1
$\sqrt{2}$
$\sqrt{3/2}$
-2 -1 0 1 2
F=2

FIG. 21 (b)

Fig. 21. Data (a) for the D_2 transition with linearly polarized light in zero magnetic field. Pulse breakup is seen to be sharp as predicted. Transitions between the ground and excited states are no longer distinct (b) in zero magnetic field. However a representation is chosen in which all transitions are distinct and have identical transition dipole moments.

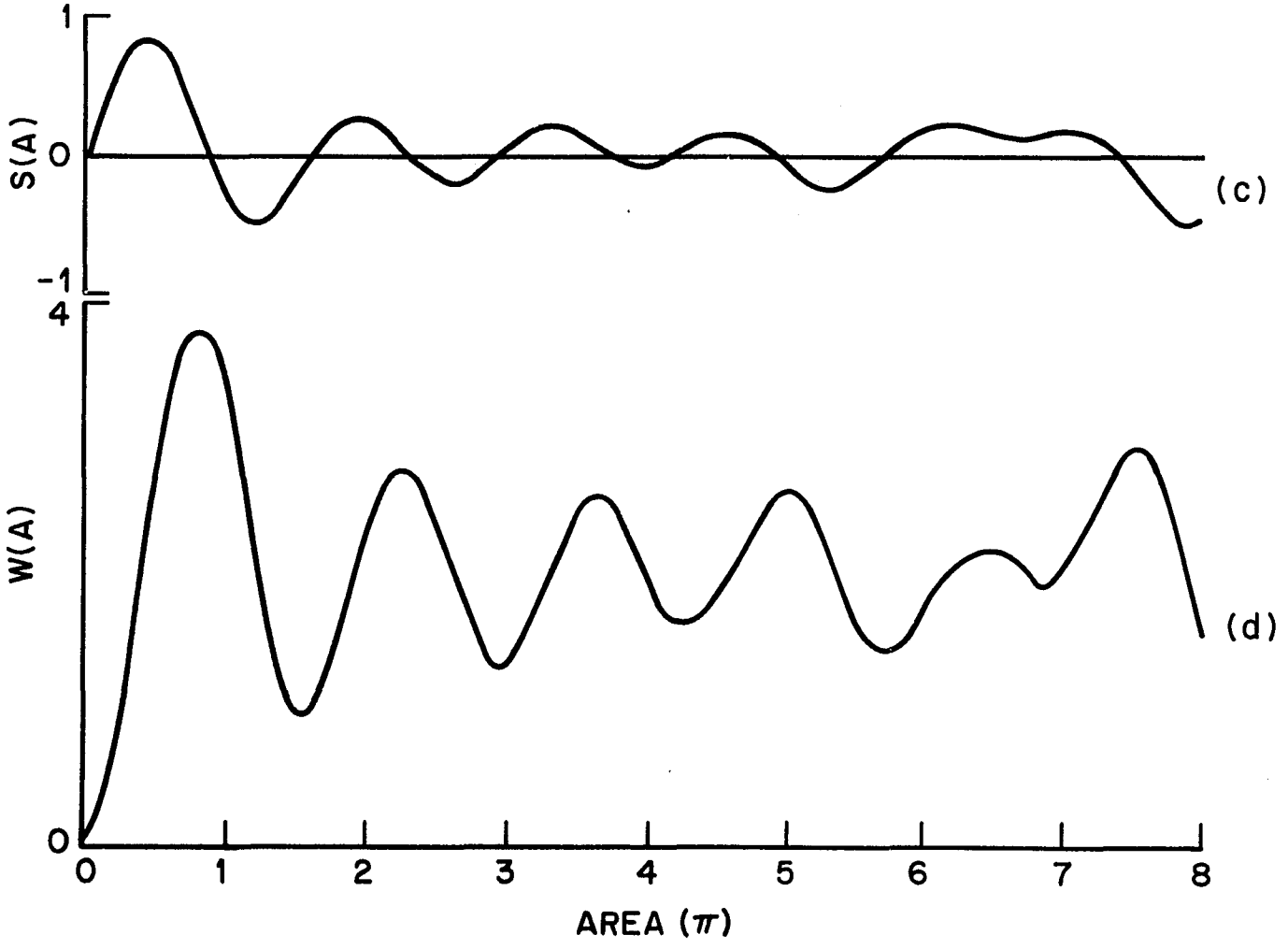

FIG. 20 (c AND d)

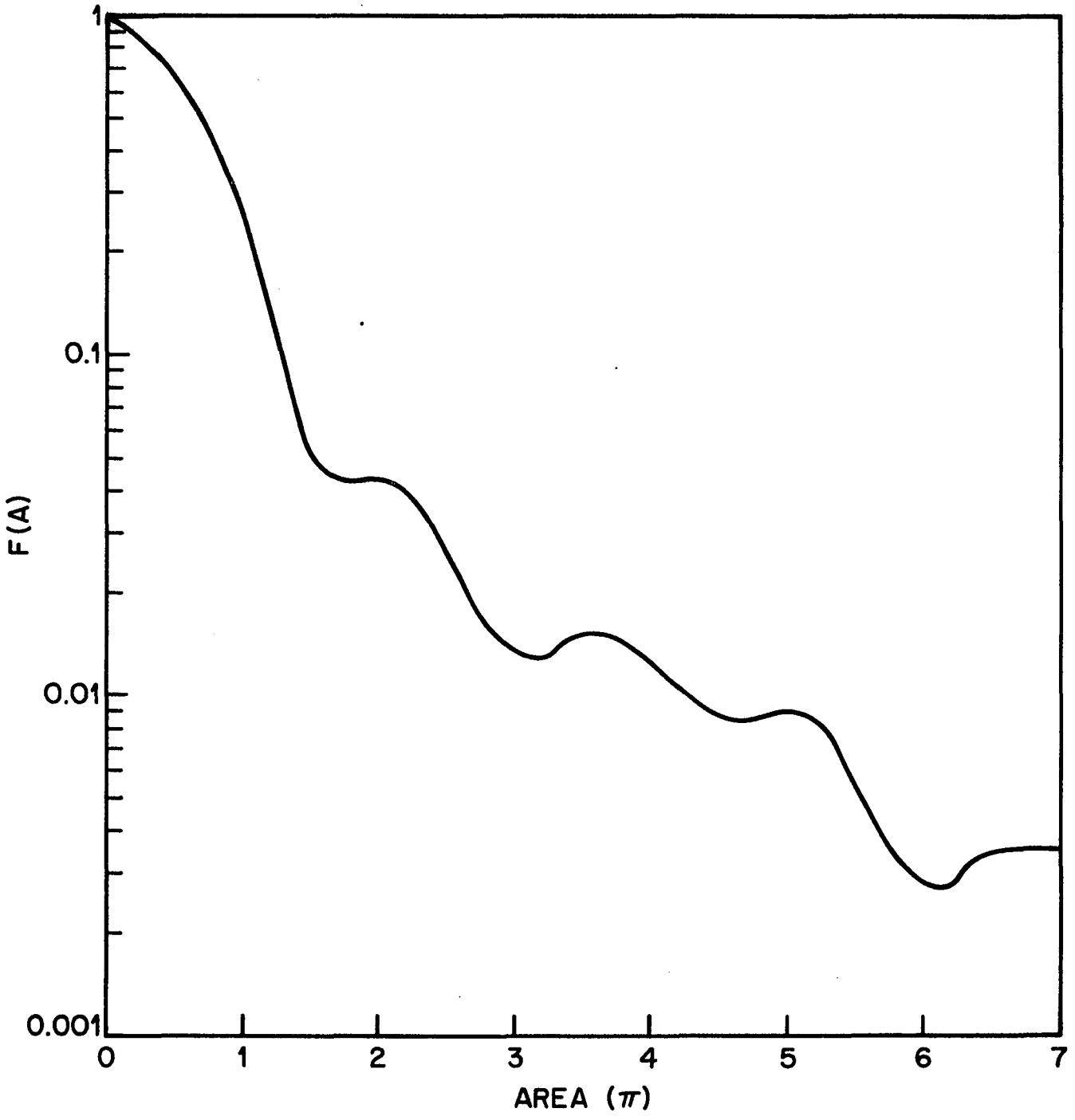

FIG. 20(e)

Fig. 22. The functions S(A), F(A), and W(A) are plotted for a single nondegenerate transition dipole, such as, the D_1 or D_2 transition dipole for linearly polarized light parallel to a large magnetic field.

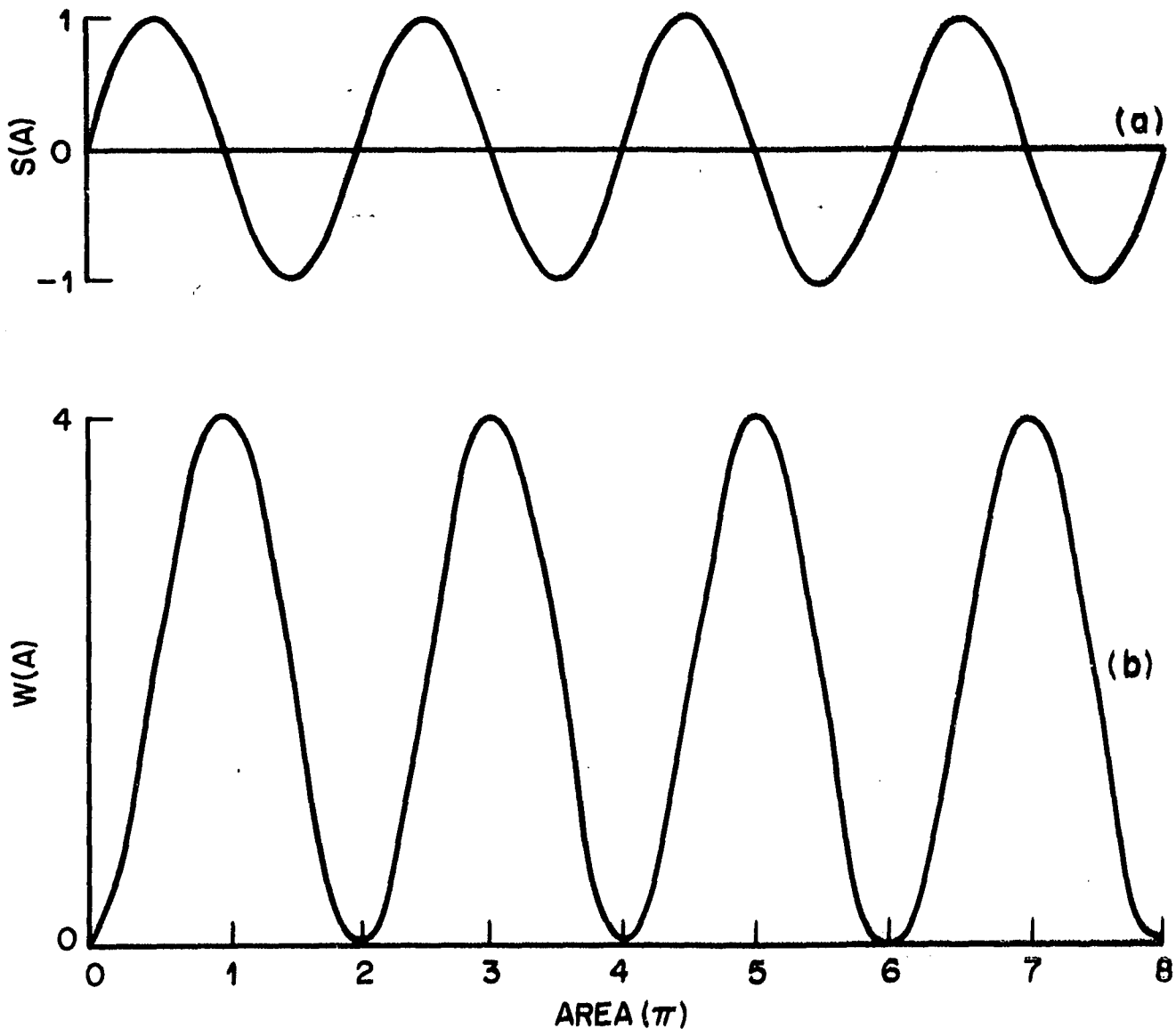

FIG. 22 (a AND b)

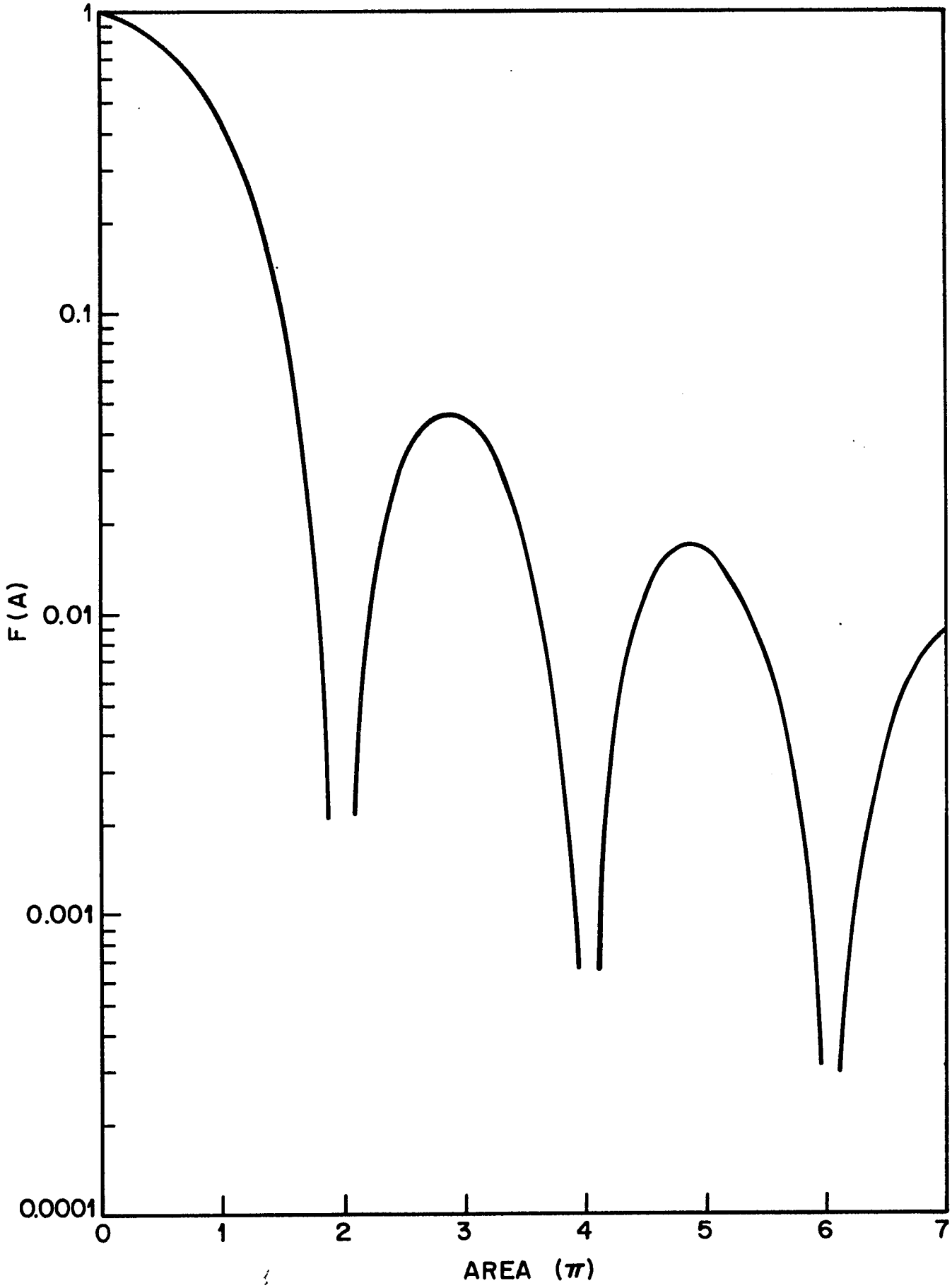

FIG. 22 (C)

Table 1

D_1 Transition Dipoles in Zero Magnetic Field Relative to the D_1 Transition Dipole Moment in a Large Magnetic Field for Light Linearly Polarized Along the Field

F	p_i	g_i
1	$\sqrt{3/4}$	2
1	1	1
1	$\sqrt{1/4}$	2
2	$\sqrt{3/4}$	2
2	1	3
2	$\sqrt{1/4}$	2

Table 2

D_2 Transition Dipoles in Zero Magnetic Field Relative to the D_1 Transition Dipole Moment in a Large Magnetic Field for Light Linearly Polarized Along the Field

F	p_i	g_i
1	$\sqrt{3/2}$	2
1	1	2
1	$1/\sqrt{2}$	2
2	$\sqrt{2}$	2
2	$\sqrt{3/2}$	2
2	1	2
2	$\sqrt{1/2}$	2